Supporting Information

DNA Mimics of Red Fluorescent Proteins (RFP) Based on G-quadruplex-confined Synthetic RFP Chromophores

Guangfu Feng[1], Chao Luo[1], Haibo Yi[1], Lin Yuan[1], Bin Lin[4], Xingyu Luo[1], Xiaoxiao Hu[2], Honghui Wang[3], Chunyang Lei[1], Zhou Nie[1,*], and Shouzhuo Yao[1]

[1]State Key Laboratory of Chemo/Biosensing and Chemometrics, College of Chemistry and Chemical Engineering, [2]Molecular Science and Biomedicine laboratory, and [3]College of Biology, Hunan University, Changsha 410082, P. R. China.
[4]Pharmaceutical Engineering & Key Laboratory of Structure-Based Drug Design & Discovery, Ministry of Education,Shenyang Pharmaceutical University, Shenyang 110016, P. R. China

*E-mail address: niezhou.hnu@gmail.com. Tel.: +86-731-88821626; Fax: +86-731-88821848

Table of Content

1. Supplemental Tables and Figures

1.1 Supplemental Tables.

Table S1. Sequences and secondary structures of the oligonucleotides used in this study.

Oligonucleotide	Sequence (5' - 3')	Structure type
NG16	GGGTGGGTTGGGTGGG	Parallel G4
EAD	CTGGGTGGGTGGGTGGGA	Parallel G4
TT_3T	GGGTGGGTTTGGGTGGG	Parallel G4
TBA	GGTTGGTGTGGTTGG	Antiparallel G4
Hum21	GGGTTAGGGTTAGGGTTAGGG	Hybrid G4
h-Telo	AGGGTTAGGGTTAGGGTTAGGGT	Hybrid G4
HT	TTGGGTTAGGGTTAGGGTTAGGGA	Hybrid G4
PW17	GGGTAGGGCGGGTTGGG	Anti- (Pb^{2+}) or parallel (K^+) G4
Ds26	CAATCGGATCGAATTCGATCCGATTG	Duplex
Ds17-1	CCAGTTCGTAGTAACCC	Double strand
Ds17-2	GGGTTACTACGAACTGG	
A21	AAAAAAAAAAAAAAAAAAAA	Single strand
T21	TTTTTTTTTTTTTTTTTTTT	Single strand

Table S2. Quantum yield (Q.Y.) of HBI and DFHBI in the presence of different molar equivalents of NG16.

Probe	Q.Y.					
	0	1 eq.	5 eq.	10 eq.	20 eq.	50 eq.
HBI[a]	~0.0004	~0.0004	~0.0004	~0.0005	~0.0006	~0.0008
DFHBI	0.0007	0.0007	0.0007	0.0008	0.0009	0.0011

[a]The concentrations of HBI and DFHBI are 1 μM.

Table S3. Quantum yield (Q.Y.) of HBI and DFHBI after binding different kinds G4 oligonucleotides.

Probe	Q.Y.						
	NG16[b]	EAD	TT3T	TBA	Hum21	h-Telo	HT
HBI[a]	~0.0006	~0.0005	~0.0007	~0.0005	~0.0005	~0.0005	~0.0006
DFHBI	0.0009	0.0008	0.0009	0.0007	0.0007	0.0007	0.0007

[a]The concentrations of HBI and DFHBI are 1 μM

[b]The concentrations of G4 oligonucleotides are 20 μM.

Table S4. Photophysical properties of RFPs and RFP mimics.

FPs /RFP mimics		Ex_{max} (nm)	Em_{max} (nm)	Stoke shift (nm)	Q.Y.
RFPs/RFP mimics	TagRFP	555	584	29	0.41
	DFHBMSI-NG16	499	583	84	0.37
	DsRed-Monomer	557	592	35	0.14
	DFHBSI-NG16	503	590	87	0.31
	mRFP1	584	607	23	0.25
	DFHBFSI-NG16	513	606	93	0.39
	JRed	584	610	26	0.20
	DFHBNI-NG16	521	612	91	0.30
Far-RFP/Far-RFP mimic	mRaspberry	598	625	27	0.15
	DFHBASI-NG16	538	620	82	0.19
Near-infrared RPF/Near-infrared RFP mimic	AQ143	595	655	60	0.04
	DFHBAPBI-NG16	556	668	112	0.032

Table S5. Two-photon properties of the RFPs and RFP mimics.

Chromophore		λ_{TPA}/nm	σ(GM)	σ' (GM)
RFP mimics	DFHBMSI-NG16	750	38.6	14.3
	DFHBSI-NG16	750	37.2	11.5
	DFHBFSI-NG16	750	24.1	9.4
RFPs	mStrawberry	700	35	12
	mCherry	740	101	24
	mPlum	724	114	15

Table S6. Sequence of the oligonucleotides used in the imaging experiments.

Probe	Sequence (5' - 3')	Target cell	Control cell
reporter[a,b]	GGGTGGGTTGGGTGGGAAAAAAGGGTGGGTTGGG TGGGAAAAAATGCCTGCGAGA	N/A[c]	N/A
sgc8[d]	ATCTAACTGCTGCGCCGCCGGGAAAATACTGTACG GTTAGAAAAAAATCTCGCAGGCA	CCRF-CEM Ramos-PTK7	Ramos
SL1	ATCAGGCTGGATGGTAGCTCGGTCGGGGTGGGTG GGTTGGCAAGTCTGATAAAAAATCTCGCAGGCA	A549	HepG2
SYL3C	CACTACAGAGGTTGCGTCTGTCCCACGTTGTCATG GGGGGTGGCCTGAAAAAATCTCGCAGGCA	HT29	HEK-293T
Random	TTGGAGTCAATCGGATGTAGGATGGTCTCCAGACA CGGGGCAAAAAA	N/A	N/A

[a]The red text is the sequence of NG16.
[b]The blue text is the linker sequence for hybridization.
[c]Not applicable.
[d]The green text is the sequence of aptamer.

1.2 Supplemental Figures.

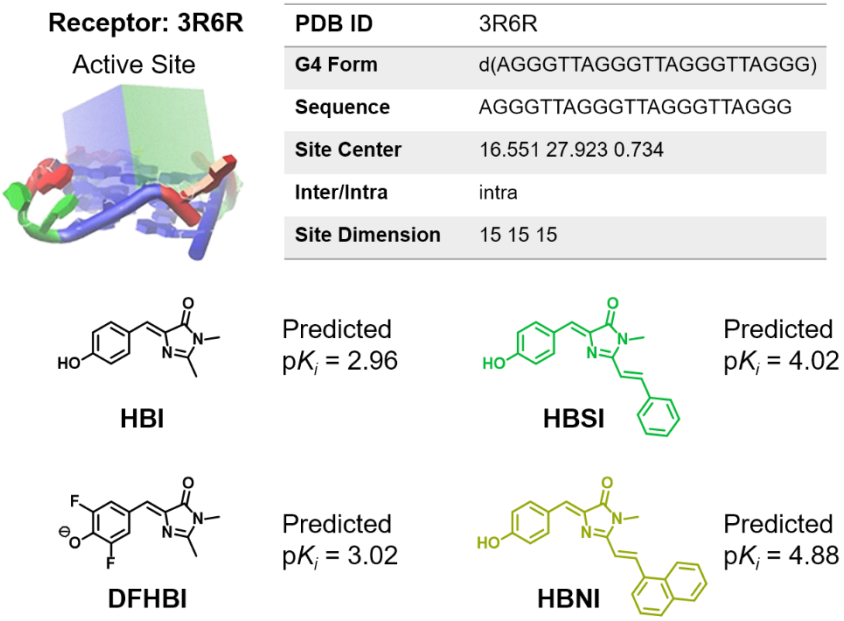

Figure S1. Theoretical prediction of molecular interactions between the chromophores and G-quadruplexes by online molecular docking system of the G-quadruplex Ligands Database (G4LDB: www.g4ldb.org).

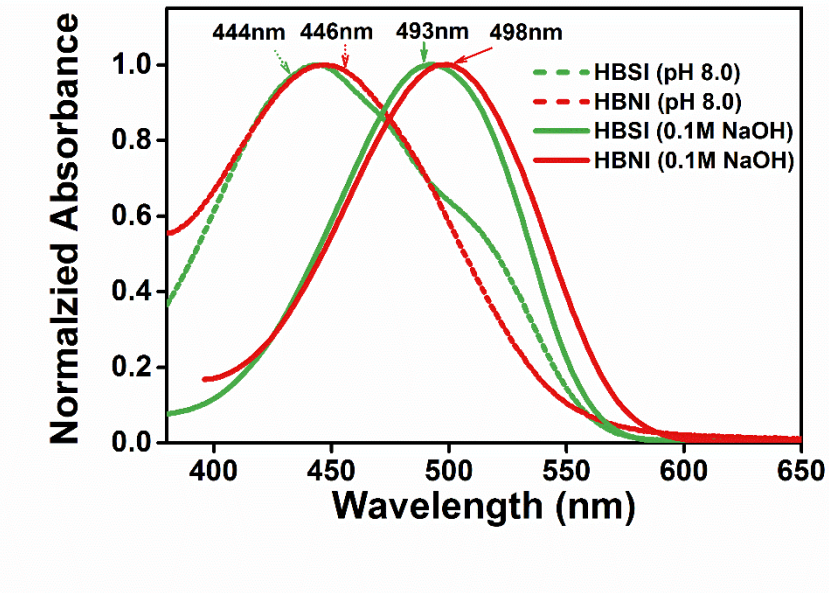

Figure S2. Normalized absorption spectra of HBSI (20 μM) and HBNI (20 μM) in aqueous solution with different pH values.

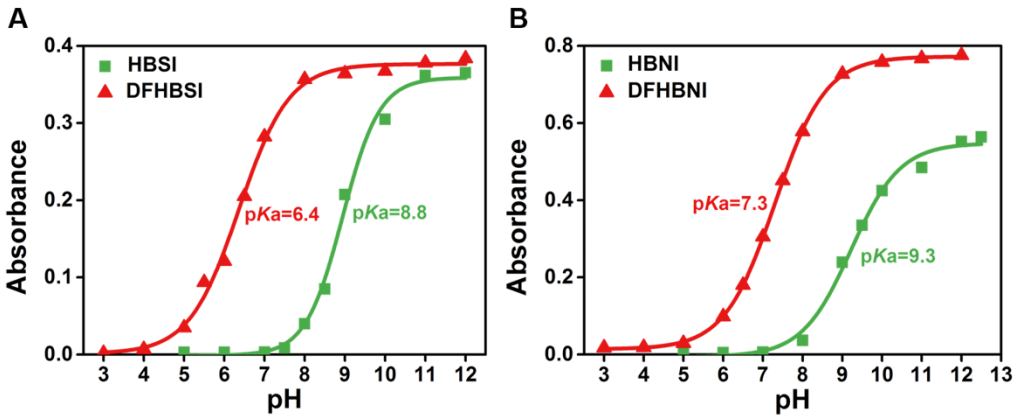

Figure S3. pK_a measurements of the chromophores. (A) HBSI and DFHBSI. (B) HBNI and DFHBNI. The concentrations of the chromophores are 20 μM.

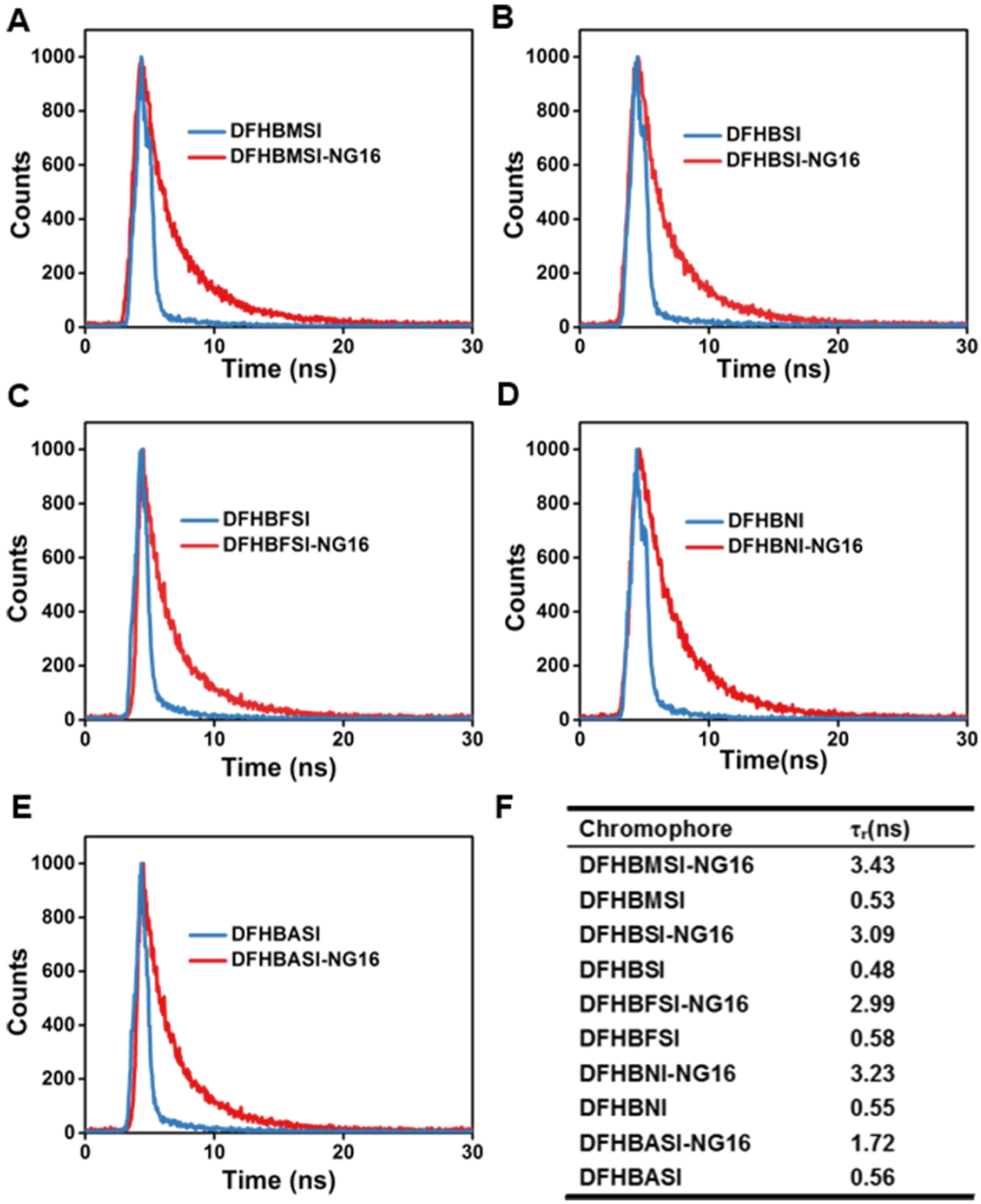

Chromophore	τ_r(ns)
DFHBMSI-NG16	3.43
DFHBMSI	0.53
DFHBSI-NG16	3.09
DFHBSI	0.48
DFHBFSI-NG16	2.99
DFHBFSI	0.58
DFHBNI-NG16	3.23
DFHBNI	0.55
DFHBASI-NG16	1.72
DFHBASI	0.56

Figure S4. Fluorescence lifetime of the RFP analogues (3 μM) in the presence and absence of NG16 (15 μM). (A) DFHBMSI, (B) DFHBSI, (C) DFHBFSI, (D) DFHBNI, (E) DFHBASI，and (F) lifetime values of the RFP analogues.

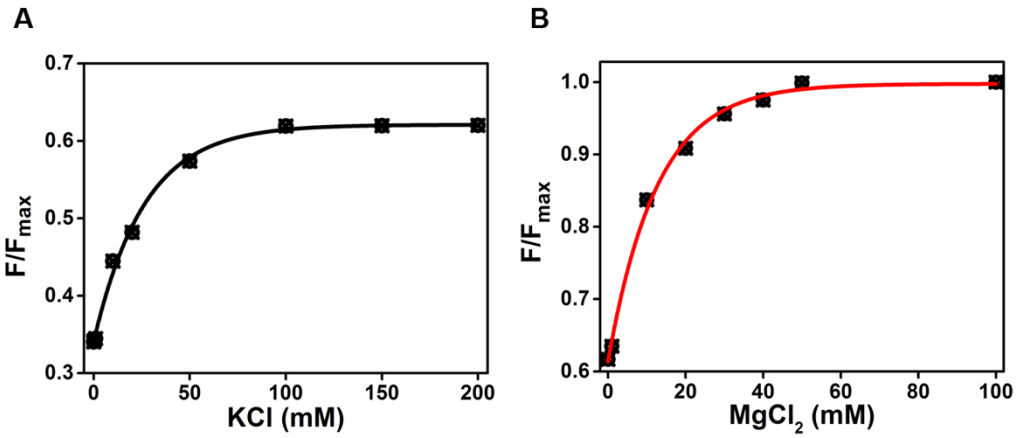

Figure S5. Effects of the concentration of (A) K^+ and (B) Mg^{2+} on the fluorescence of DFHBFSI-NG16 complex (3 μM). *F* is the fluorescence intensity of DFHBFSI-NG16 at 606 nm in the presence of K^+ or Mg^{2+}, and F_{max} is the fluorescence intensity of DFHBFSI-NG16 at 606 nm in Tris-HCl buffer (25 mM Tris, 100 mM KCl, 50 mM $MgCl_2$ and pH 8.0).

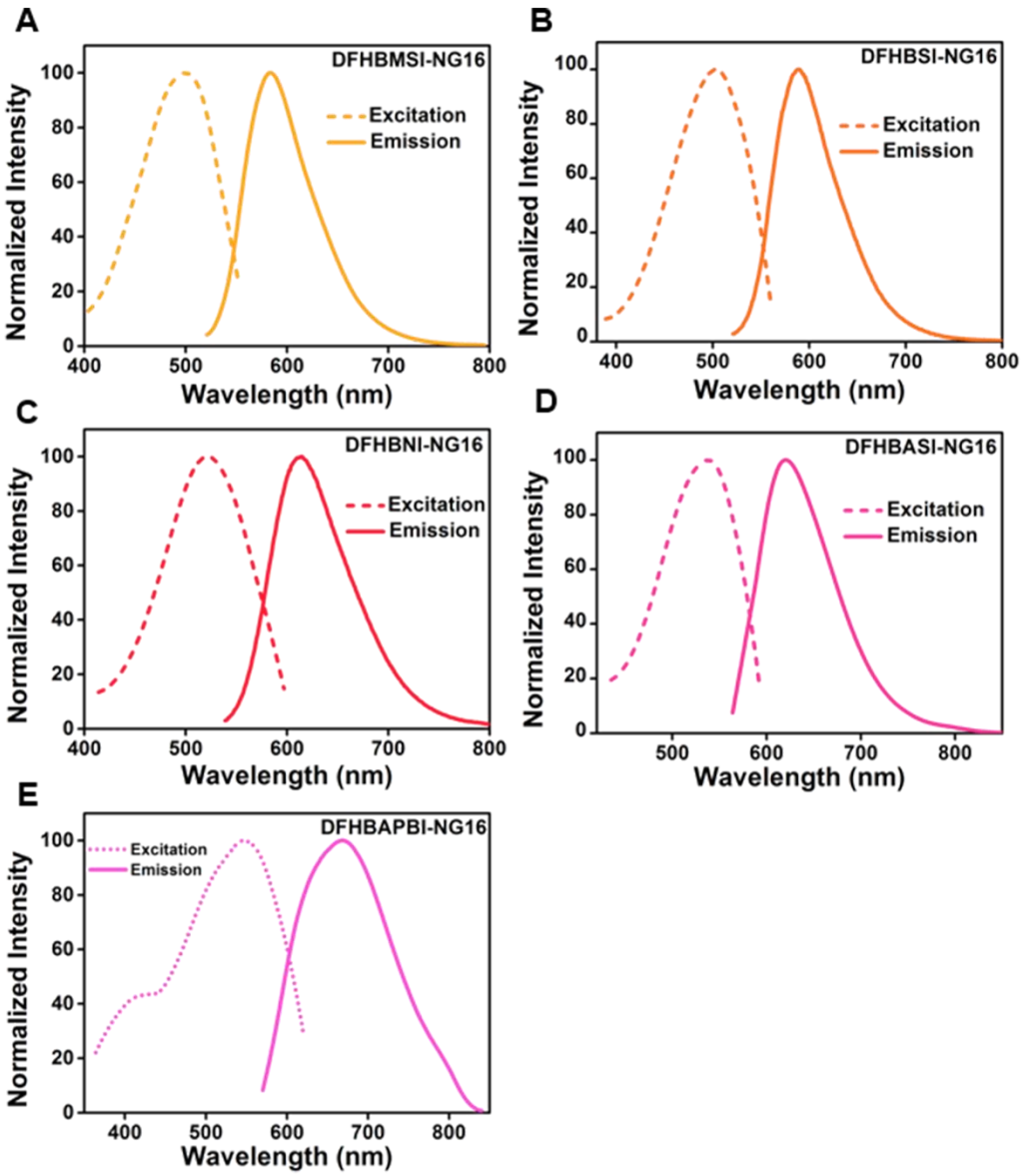

Figure S6. Normalized excitation and emission spectra of the chromophore-NG16 complexes (3 μM) in Tris-HCl buffer (25 mM Tris, 100 mM KCl, 50 mM $MgCl_2$ and pH 8.0). (A) DFHBMSI-NG16, (B) DFHBSI-NG16, (C) DFHBNI-NG16, (D) DFHBASI-NG16 and (E) DFHBAPBI-NG16 Complex.

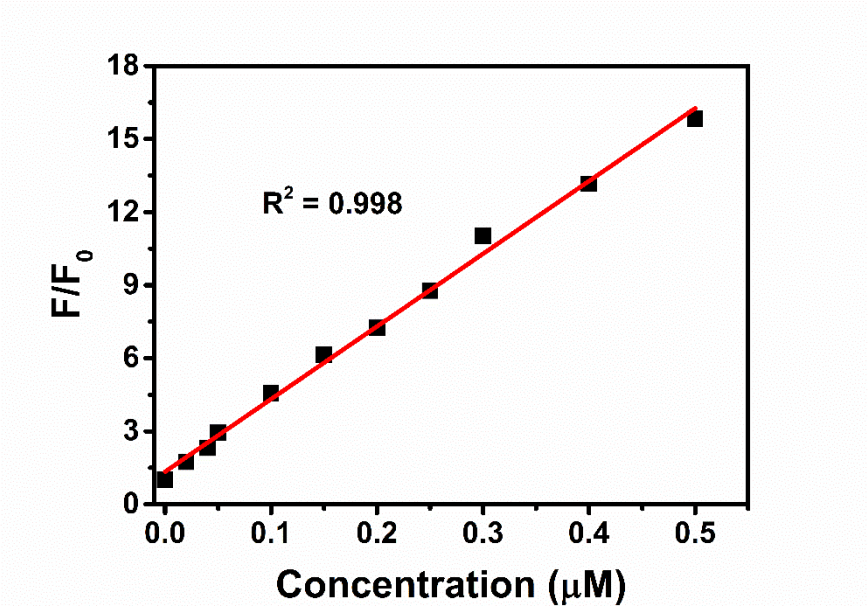

Figure S7. Calibration curve of DFHBFSI-based assay for the detection of NG16 (0.02 – 0.5 μM) in Tris-HCl buffer (25 mM Tris, 100 mM KCl, 50 mM $MgCl_2$ and pH 8.0). DFHBFSI, 3 μM.

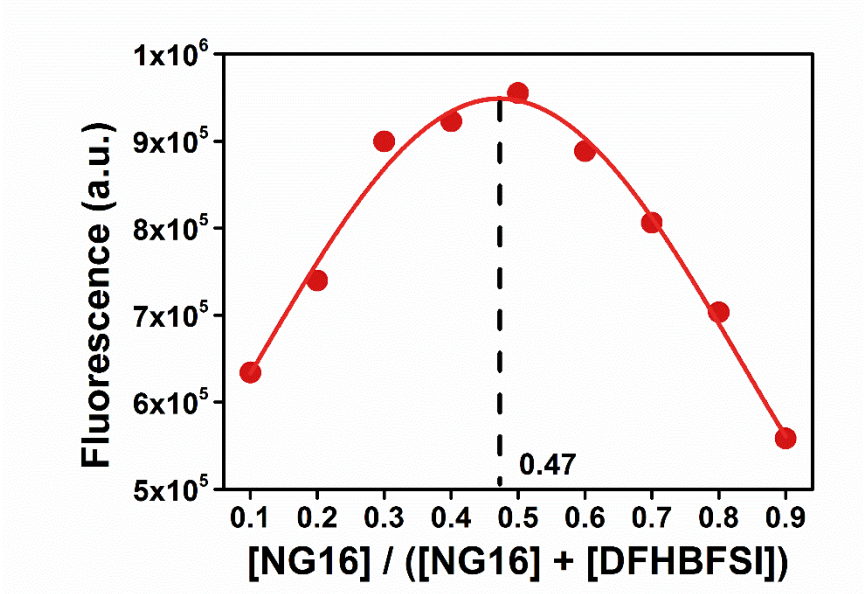

Figure S8. Job's plot obtained from fluorometric analysis of the mixtures of DFHBFSI with NG16 in Tris-HCl buffer (25 mM Tris, 100 mM KCl, 50 mM $MgCl_2$ and pH 8.0). X-axis, mole fraction of NG16. The total concentration of DFHBFSI and NG16 is 3 μM.

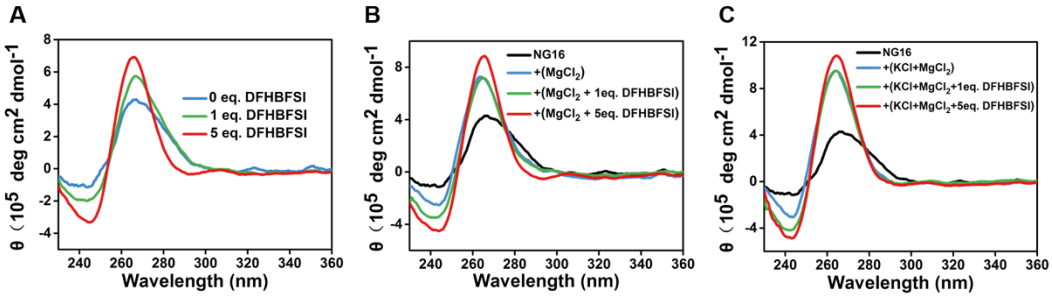

Figure S9. CD spectra of NG16 (10 μM) at different conditions. (A) CD spectra of NG16 with different equivalents of DFHBFSI in Tris-HCl buffer (25 mM, pH 8.0). (B) CD spectra of (A) in the presence of Mg^{2+}. (C) CD spectra of (B) with the existence of K^{+}. $MgCl_2$, 50 mM; KCl, 100 mM.

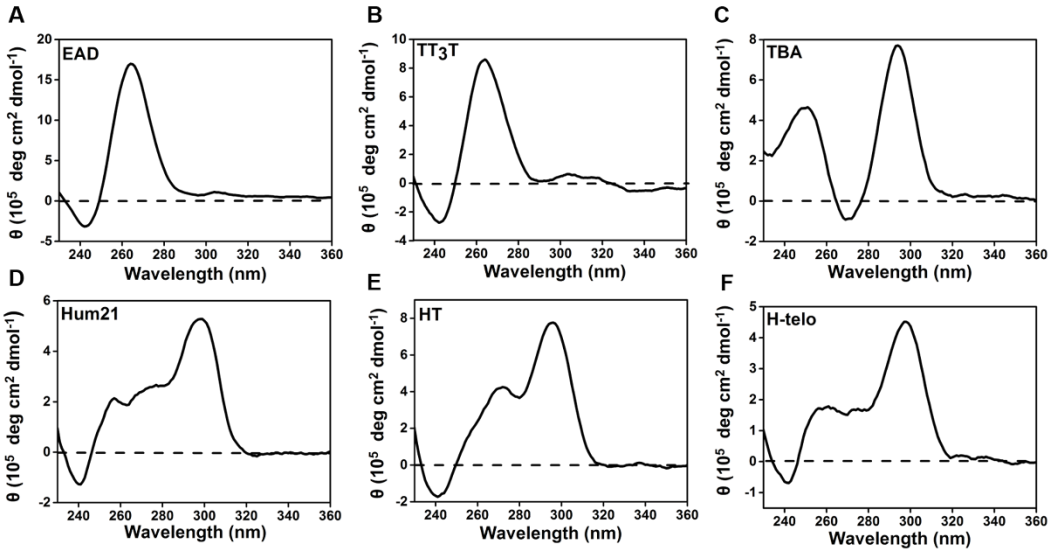

Figure S10. CD spectra of various G4 oligonucleotides in Tris-HCl buffer (25 mM Tris, 100 mM KCl, 50 mM $MgCl_2$ and pH 8.0). (A) EAD, (B) TT_3T, (C) TBA, (D) Hum21, (E) HT and (F) H-telo. Concentrations of G4 oligonucleotides are 10 μM.

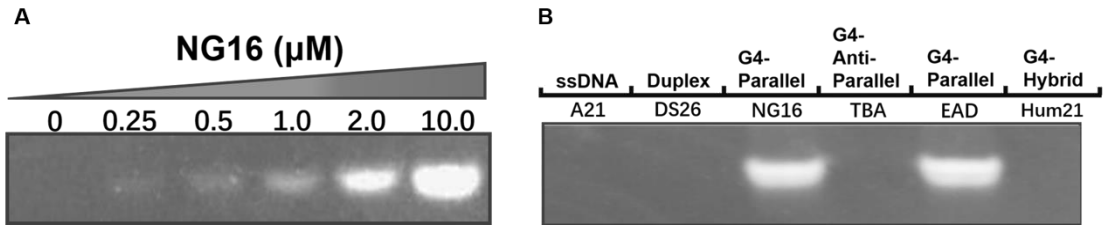

Figure S11. Native polyacrylamide electrophoresis of (A) various amounts of NG16 and (B) different G4 oligonucleotides (10 μM) stained by DFHBFSI (2 μM).

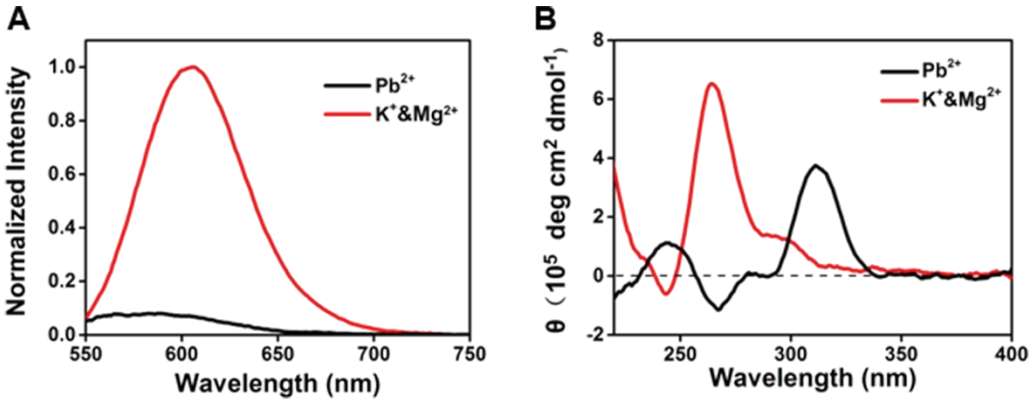

Figure S12. (A) Fluorescence emission spectra and (B) CD spectra of DFHBFSI/PW17 in the presence of K^+&Mg^{2+} or Pb^{2+}. DFHBFSI, 1 μM; PW17, 5 μM; K^+, 10 mM; Mg^{2+}, 50 mM; Pb^{2+}, 10 μM.

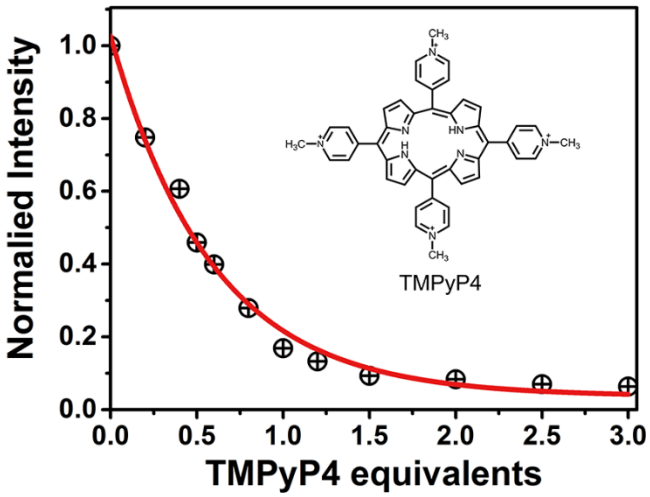

Figure S13. Fluorescence intensity of DFHBFSI-NG16 at 606 nm upon the addition of various amount of TMPyP4 (0 – 9 μM) in Tris-HCl buffer (25 mM Tris, 100 mM KCl, 50 mM $MgCl_2$ and pH 8.0). DFHBFSI, 3 μM; NG16, 3 μM.

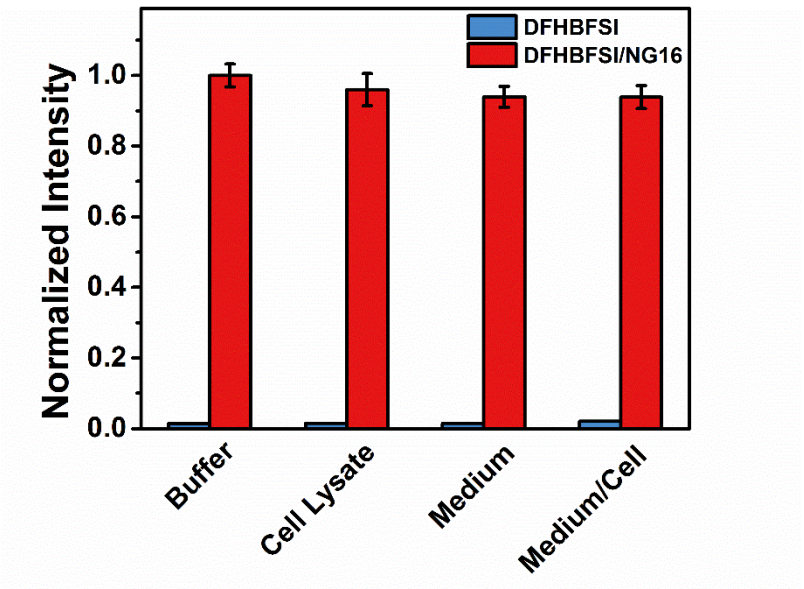

Figure S14. Fluorescence intensity of DFHBFSI and DFHBFSI-NG16 at 606 nm in buffer, cell lysate, medium, and medium with cells. Buffer: 25 mM Tris, 100 mM KCl, 50 mM $MgCl_2$ and pH 8.0. Cell lysate: 30000 cell/mL of CCRF-CEM in PBS (10 mM, pH 8.0) with 100 mM KCl and 50 mM $MgCl_2$. Medium: RPMI 1640 (pH 8.0) with 100 mM KCl and 50 mM $MgCl_2$. Medium with cell: Medium with 30000 cell/mL of CCRF-CEM.

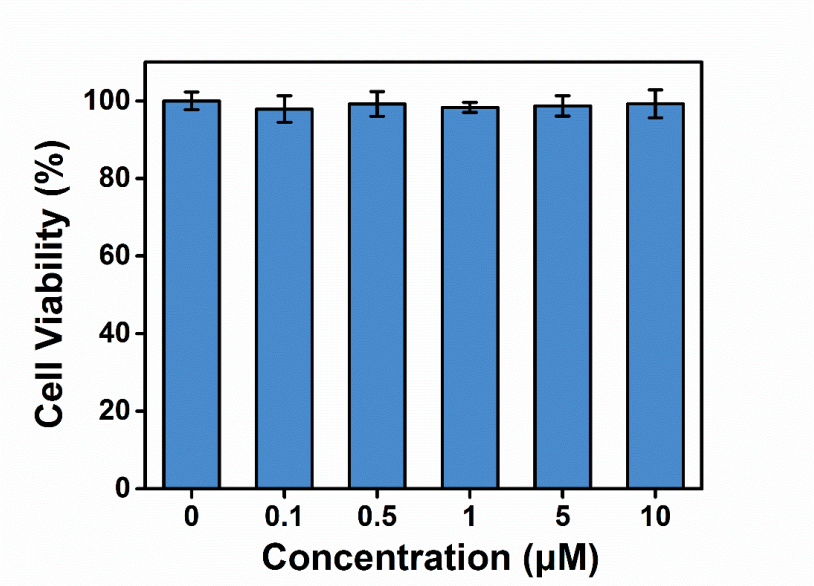

Figure S15. Cell viability of DFHBFSI were measured in CCRF-CEM cells by CCK-8 assay. CCRF-CEM cells were treated with DFHBFSI (concentration ranges from 0 to 10 μM) for 24 h. (In the imaging section, 0.5 μM of DFHBFSI was used in the experiments. Therefore, it is reasonable to stop at 10 μM, 20 times the concentration used in the experiments).

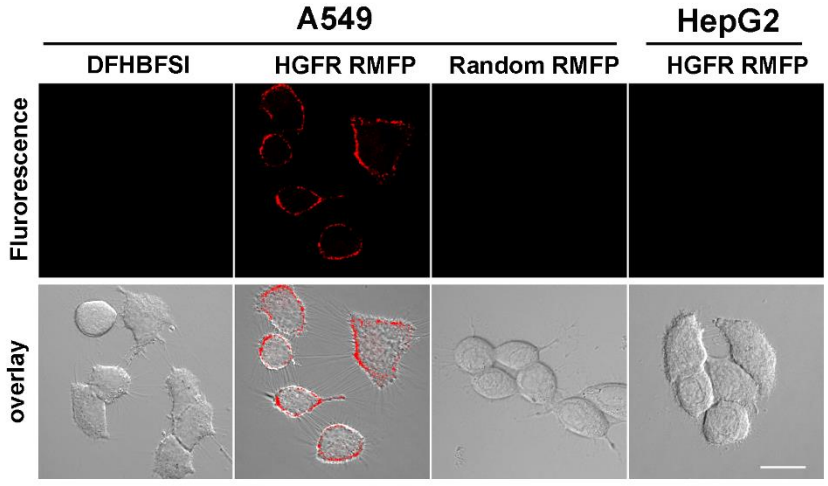

Figure S16. Confocal microscope image of HGFR RMFP treated A549 cells and HepG2 cells at 570 – 620 nm channel (top) and overlay images of fluorescence channel and bright-field channel (bottom), Scale bar: 10 μm.

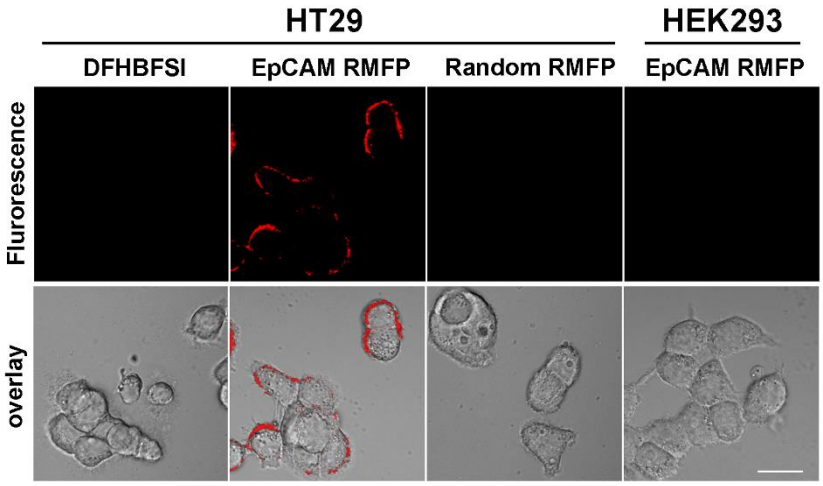

Figure S17. Confocal microscope image of EpCAM RMFP treated HT29 cells and HEK293 cells at 570 – 620 nm channel (top) and overlay of fluorescence channel and bright-field channel (bottom), Scale bar: 10 μm.

2. General Experimental Procedures.

2.1 Measurement of Two-photon Cross Section.

The two-photon cross section (σ) was determined by using a femtosecond (fs) fluorescence measurement technique. DFHBMSI (3 μM), DFHBSI (3 μM) or DFHBFSI (3 μM) was mixed with NG16 (15 μM) in Tris-HCl buffer (25 mM Tris, 100 mM KCl, 50 mM $MgCl_2$ and pH 8.0), and then the two-photon fluorescence spectrum of the sample was measured from 710 nm to 870 nm by using Rhodamine 6G in MeOH (σ = 70 GM at 810 nm) as the standard. The two-photon cross-section was calculated by using the Equation S1,[1]

$$\sigma = \sigma_r(F_t n_t^2 \Phi_r C_r) \,/\, (F_r n_r^2 \Phi_t C_s) \qquad \text{(S1)}$$

where the subscripts *t* and *r* stand for the sample and reference molecules. F is the average fluorescence intensity integrated from 2PE spectrum; *n* is the refractive index of the solvent; *C* is the concentration; Φ is the quantum yield, and σ_r is the two-photon cross-section of the reference molecule.

2.2 p*K*a Measurements.

For the p*K*a measurement, HBSI (20 μM) was prepared in buffer with pH range of 5 – 12, and then absorbance values at 493 nm were measured. Similarly, for the p*K*a measurements of DFHBSI, HBNI and DFHBNI (20 μM), the pH ranges of buffer solutions were 3 – 12, 5 – 12 and 3 – 12, and absorbance values at 503 nm, 496 nm and 520 nm were recorded, respectively. The half-maximal value of the chromophores was calculated based on the plot of absorbance value versus pH.

2.3 Quantum Yield Calculations.

The quantum yield was calculated using the Equation S2,[2]

$$\Phi_{F(X)} = \Phi_{F(S)}(n_X \,/\, n_S)^2 A_S F_X \,/\, (A_X F_S) \qquad \text{(S2)}$$

where Φ_F is the fluorescence quantum yield; *A* is the absorbance at the excitation wavelength; *F* is the area under the corrected emission curve, and *n* is the refractive

index of the solvent. Subscripts S and X refer to the standard and the unknown, respectively. The solutions of synthesized RFP chromophore analogues, rhodamine 6G, Cy5 and standards were kept absorptions below 0.05.

2.4 Dissociation Constant Measurements.

The K_d of RFP analogues to the respective G-quadruplexes were analyzed by one site specific binding model based the Equation S3.[3]

$$Y = Y_{max}X / (K_d + X) \qquad (S3)$$

Where Y represents the fluorescence fold change of RFP analogues; Y_{max} is the fluorescence fold change of RFP analogue when saturated with G-quadruplex, and X is the concentration of the G-quadruplex (NG16).

2.5 Photo-bleaching Analysis

Aqueous droplets of Lyso-Tracker Red (1 μM), mCherry (1 μM), and DFHBFSI-NG16 (1 μM) were formed under mineral oil in a chamber on the fluorescence microscope stage. Photo-bleaching experiments were performed on the Nikon confocal microscope with 20 mW solid-state laser for 60 min. Fluorescent Images were captured every 8 s with the camera through 10 X objective lens and analyzed by the ROI analysis of NIS-element viewer.

2.6 Molecular Modeling.

The coordinates of parallel G-quadruplex NG16 (PDB ID: 2LXV) were retrieved from Protein Data Bank.[4,5] 2LXV is dimeric and only the first chain was used. NG16 and the phenolate form of DFHBFSI were prepared by AutDockTools and molecular interactions between them were studied by docking simulations via AutoDock 4.2.6 with the Lamarckian genetic algorithm.[6] Since it is possible for DFHBFSI to interact with NG16 via end stacking at either the 3’ end or 5’ end and groove-binding at all four sides, the most energetically favorable binding mode was adopted as the starting conformation for each possible binding mode for the following Molecular Dynamics (MD) simulations. The phenolate DFHBFSI without G-quadruplex was also simulated

for comparison. There are seven simulations in total (the DFHBFSI alone, the 3' end stacking simulation, 5' end stacking simulation, the side1, side2, side3 and side4 simulations for the groove binding simulations). The force field parameters of phenolate DFHBFSI were developed by following the CGenFF protocols and the c36 version of CHARMM DNA force field parameters were used for G-quadruplex.[7,8] Each system was then solvated using TIP3P water molecules, which were extended up to 10 Å in a rectangular box. The systems were neutralized by adding K^+ ions. The solvated systems were subjected to equilibration followed by 100 ns of MD run with coordinates saved for every 10 picoseconds. The coordinates of hybrid G4 HT and antiparallel G4 TBA were retrieved based on PDB ID 2GKU and 5MJX.[9,10] The binding modes of DFHBFSI with these two G-quadruplexes were studied in the same protocol as 2LXV. The binding free energies between the DFHBFSI ligand and the G-quadruplex were calculated by MM/PBSA (8) method in CHARMM.[11] All the figures were rendered using PyMOL 1.3.[12]

2.7 DFT Calculations.

The density functional theory method with CAM-B3LYP method was applied to the geometry optimization of DFHBFSI complex with 6-311++G** basis set.[13,14] Time dependent density functional theory (TDDFT) is one of the most popular approaches for the calculation of excitation energies in quantum chemistry because of its efficiency and accuracy[15,16]. Since conventional TDDFT calculations underestimate charge-transfer excitation energies, long-range-corrected TDDFT (LRC-TDDFT) method was employed with CAM-B3LYP functional and 6-311++G** basis set. Potential energy surfaces of S1 and S0 along the phenoxy-twisted photoisomerization pathway were carried out at the LRC-TDDFT/6-311++G** level. The rotation step is 5 ºin the range of 0 º– 90 º, and 10 ºafter 90 º. Coordinate-driving potential surface scans were generated by fixing the bridge dihedral angle (Figure 5A) and minimizing all other degrees of freedom subject to this constraint. All geometry optimization and potential energy surface calculations were performed with the Gaussian 09 software package.[17] Based on results of Mulliken charge population analyses, the spatial distribution of electron

density was visualized using the program VMD (version 1.9.1).[18]

2.8 Cell Culture.

CCRF-CEM, Ramos and A549 cells were cultured in RPMI 1640 (Hyclone) with 10% fetal bovine serum (Gibco), 100 U/mL penicillin and 100 ug/mL streptomycin (Hyclone). HepG2、HEK-293T cells were cultured in the high glucose (4.5 g/L) version of DMEM (Hyclone) supplemented with 10% fetal bovine serum, 100 U/mL penicillin and 100 ug/mL streptomycin. HT-29 cells were cultured in McCoy's 5a Medium Modified (Hyclone) supplemented with 10% fetal bovine serum, 100 U/mL penicillin and 100 ug/mL streptomycin. All cells were maintained at 37 °C in a 5% CO_2 atmosphere.

2.9 Cytotoxicity Measurements.

Cytotoxicity of DFHBFSI was determined by CCK-8 assays. Before the experiment, 3×10^4 CCRF-CEM cells were seeded in wells of a 96-well plate (Costar) and incubated with various concentrations of DFHBFSI in RPMI 1640 medium supplemented with 10% fetal bovine serum in a humidified incubator containing CO_2 (5%) at 37 ℃. The medium was removed after 24 h and replaced with a mixture containing 100 μL of fresh RPMI 1640 and 10 μL of CCK-8 reagent solution (Bimake, Shanghai). After 1 h incubation, the absorbance of the solution at 450 nm was measured using a TECAN Infinite M200 PRO plate reader.

2.10 Construction of Plasmids and Real-time Quantitative Reverse Transcription PCR

Gene sequences of EGFP and PTK7 were PCR amplified and cloned into a pCDN3.1 backbone to obtain plasmids pCDN3.1-*egfp* and pCDN3.1-*ptk7*, respectively. The reconstructed pCDN3.1-*egfp* was transformed into CCRF-CEM by electric stock, and the transfected CCRF-CEM cells with pDisplay-EGFP were used for a co-localization analysis. The pCDN3.1-*ptk7* was transformed into Ramos cells to obtained transfected Ramos cells (Ramos-PTK7).

Ramos cells, Ramos cells transfected by pCDN3.1, and Ramos cells transfected pCDN3.1-*ptk7* were cultured in RPMI 1640 medium supplemented with 10% fetal bovine serum in a humidified incubator containing CO_2 (5%) at 37 ℃ for 48 h. Then total RNA of 1×10^6 cells was extracted by a RNAprep Pure Cell/Bacteria Kit (Tiangen, China) according to the manufacturer's instruction. The relative mRNA levels of PTK7 in the cells were determined by quantitative reverse transcription. Primers: ptk7-F, 5'-AGCGGAGACAGGATGTCAAC-3'; ptk7-R: 5'-CTGGACATGGGCACGAATCT-3'.

2.11 Flow Cytometry and Confocal Laser Scanning Microscopy Assay

The sgc8 probe (500 nM) was incubated with 5×10^5 CCRF-CEM cells or Ramos cells in DPBS for 30 min, and washed by 0.2 mL DPBS twice. Then, the cells were incubated with reporter probe (500 nM) and DFHBFSI (500 nM) in buffer (DPBS with 10 mM KCl and 30 mM $MgCl_2$) for 10 min. After that, the sample was washed and re-dispersed by 0.2 mL DPBS with 10 mM KCl and 30 mM $MgCl_2$. The above steps were performed at 4 ℃. Finally, the cells were subjected to flow cytometry (Beckman Coulter Gallios，USA) at RT, and the data was obtained by counting 20000 events.

Cells (5×10^5) were incubate with their corresponding aptamer probes (500 nM of sgc8, SL1 or SYL3C) in DPBS for 30 min, and washed by 0.2 mL DPBS twice. After that, the cells were incubated with reporter probe (500 nM) and DFHBFSI (500 nM) in buffer (DPBS with 10 mM KCl and 30 mM $MgCl_2$) for 10 min. The steps prior to confocal imaging were performed at 4 ℃. Then one-photon and two-photon imaging were performed on Nikon A1 and Olympus FV1000 confocal laser scanning microscopy at RT, respectively.

Co-localization of two fluorescent channels in confocal images was determined by Manders' overlap coefficient (R)[19] using the Image-Pro Plus software (Media Cybernetics. Inc). An overlap coefficient higher than 0.6 indicates strong co-localization. Values are means with SD (n = 5).

2.12 Tissue Imaging.

Frozen tissue slices were prepared from CCRF-CEM cell xenograft mice. To rule out nonspecific binding, frozen tissue slices were incubated in 1 μM random sequences for 5 min. Then, sgc8 probe (500 nM) was incubated with the sections in DPBS for 30 min. Each frozen tissue section was washed with 0.5 mL DPBS for three times. Finally, tissue section was incubated with reporter probe (500 nM) and DFHBFSI (500 nM) in buffer (DPBS with 10 mM KCl and 30 mM $MgCl_2$) for 1 h. After the incubation, the tissue section was washed with 0.5 mL buffer (DPBS with 10 mM KCl and 30 mM $MgCl_2$) three times and then observing under a fluorescence microscope.

3. Synthesis and Characterization.

3.1 Synthesis of 2, 6-difluoro-4-hydroxybenzaldehyde (1a)[20]

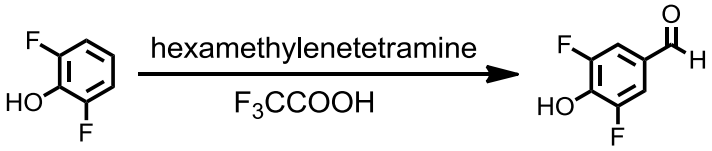

Hexamethylenetetramine (9.5 g, 67.76 mmol), 2, 6-difluorophenol (8 g, 61.6 mmol) and TFA (90 mL) were stirred at 120 ℃ under argon atmosphere for 12 h. After allowing the reaction to cool to room temperature, the solvent was removed under vacuum condition. The crude product was re-dissolved in dichloromethane, and washed by acidified ultrapure water (pH 1.0). The aqueous layer was separated, extracted with dichloromethane (3×50 mL). And the separated organic layer was dried with anhydrous magnesium sulfate and evaporated in vacuum to afford a white solid (9.7 g, yield 70%). ^{1}HNMR (400 MHz, $CDCl_3$, ppm) 9.82 (s, 1H), 7.49 (d, J = 8.0 Hz, 2H), 6.29 (s, 1H). ^{13}CNMR (100 MHz, $CDCl_3$, ppm) 189.40, 153.19, 150.73, 139.40, 127.96.

3.2 Synthesis of (Z)-2, 6-difluoro-4-((2-methyl-5-oxooxazol-4(5H)-ylidene) methyl) phenyl acetate (2a)

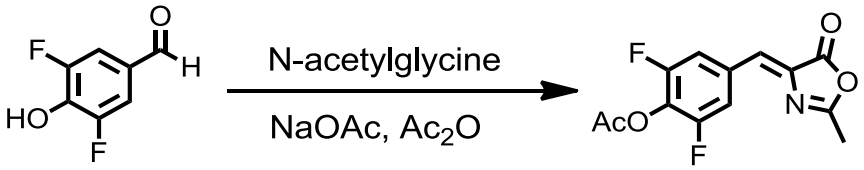

N-Acetylglycine (1.17 g, 10 mmol), anhydrous sodium acetate (0.82 g, 10 mmol), 2,6-difluoro-4-hydroxybenzaldehyde (1.58 g, 10 mmol), and acetic anhydride (10 mL) were stirred at 120 ℃ for 4 h. After allowing the reaction to cool to room temperature, the resulting crude solid was then washed with a small amount of cold ethanol, hot water dried to afford the primary product which was recrystallized from ethanol, yielding a yellow solid (2.08 g, yield 74%), without purification and characterization for the next step.

3.3 Synthesis of (Z)-4-(3, 5-difluoro-4-hydroxybenzylidene)-1, 2-dimethyl-1H-imidazol-5(4H)-one (3a)[21]

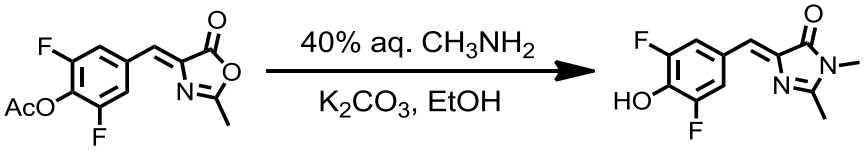

Compound **2a** (1 g, 3.56 mmol), potassium carbonate (700 mg, 5.06 mmol), 40% aqueous methylamine (2 mL), and ethanol (20 mL) were stirred at 120 ℃ for 4 h. The mixture was cooled to room temperature, the precipitate was filtered and washed briefly with cold ethanol. The precipitate was then re-dissolved in a 1:1 mixture of ethyl acetate and aqueous sodium acetate solution (500 mM, pH 3.0). The organic layer was separated, dried with anhydrous magnesium sulfate and the solvent was evaporated in vacuums to afford an orange solid (553 mg, yield 62%). ^{1}H NMR (400 MHz, CD_3OD, ppm) 7.28 (s, 1H), 7.19 (d, J = 8.0 Hz, 2H), 3.79 (s, 3H), 3.12 (s, 3H).

3.4 Synthesis of (4Z)-(3, 5-difluoro-4-hydroxybenzylidene)-2-((E)-2, 5-difluorostyryl)-1-methyl-1H-imidazol-5(4H)-one (DFHBFSI).

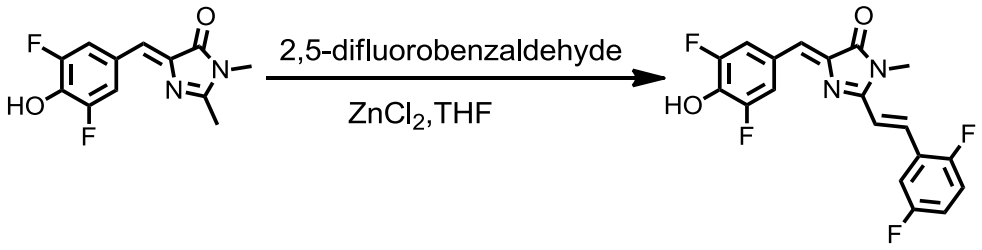

Compound **3a** (176 mg, 0.7 mmol), anhydrous zinc chloride (95 mg, 0.7 mmol), 2,5-difluorobenzaldehyde (114 mg, 0.8 mmol), and THF (15 mL) were stirred at 80 ℃ for 6 h. After allowing the reaction to cool to room temperature the crude product was purified by silica gel column chromatography (PE: EtOAc = 5:1, v/v) to afford red solid (92.1mg, yield 35%). ^{1}H NMR (400 MHz, DMSO-d_6, ppm) 7.96-7.99 (m, 4H), 7.33-7.37 (m, 3H), 6.98 (s, 1H), 3.24 (s, 3H). HRMS (ESI): m/z $[M + H]^+$ = calcd. for $C_{19}H_{13}F_4N_2O_2$ 377.0835; found 377.0832.

3.5 Synthesis of (4Z)-(3, 5-difluoro-4-hydroxybenzylidene)-2-((E)-4-methoxystyryl)-1-methyl-1H-imidazol-5(4H)-one (DFHBMSI).

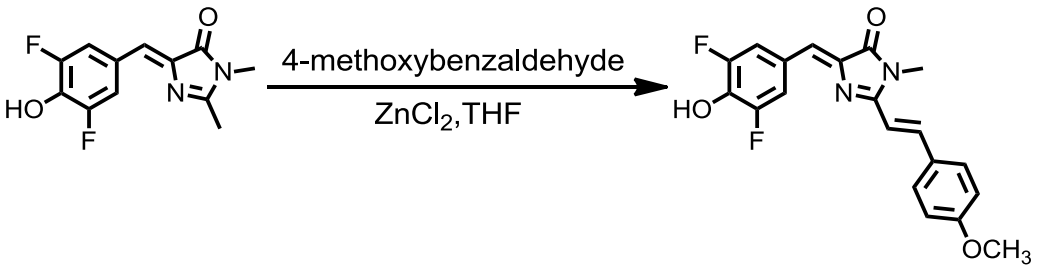

Compound **3a** (176 mg, 0.7 mmol), anhydrous zinc chloride (95 mg, 0.7 mmol), 4-methoxybenzaldehyde (108.8 mg, 0.8 mmol), and THF (15 mL) were stirred at 80 ℃ for 6 h. After allowing the reaction to cool to room temperature the crude product was purified by silica gel column chromatography (PE: EtOAc = 5:1, v/v) to afford a red solid (92.1 mg, yield 35%). ^{1}H NMR (400 MHz, DMSO-d_6, ppm) 7.95-8.04 (m, 3H), 7.85 (d, J = 8.0 Hz, 2H), 7.02-7.10 (m, 3H), 6.91 (s, 1H), 3.83 (s, 3H), 3.26 (s, 3H) ^{13}C NMR (100 MHz, DMSO-d_6, ppm), 170.36, 161.61, 161.27, 153.64, 151.24, 140.89, 139.37, 132.11, 130.78, 128.18, 122.77, 115.70, 114.92, 111.68, 55.87, 26.87. HRMS (ESI): m/z $[M + H]^+$ = calcd. for $C_{20}H_{17}F_2N_2O_3$ 371.1129; found 371.1130.

3.6 Synthesis of (4Z)-(3, 5-difluoro-4-hydroxybenzylidene)-1-methyl-2-((E)-styryl)-1H-imidazol-5(4H)-one (DFHBSI).

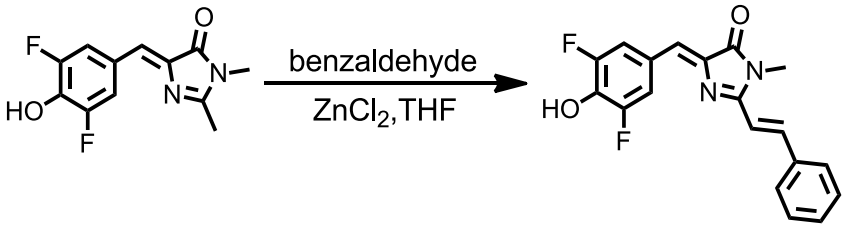

Compound **3a** (176 mg, 0.7 mmol), anhydrous zinc chloride (95 mg, 0.7 mmol), benzaldehyde (84.8mg, 0.8 mmol), and THF (15 mL) were stirred at 80 ℃ for 6 h. After allowing the reaction to cool to room temperature the crude product was purified by silica gel column chromatography (PE:EtOAc = 3:1, v/v) to afford a yellow solid (123.4 mg, yield 52%). ^{1}H NMR (400 MHz, DMSO-d_6, ppm) 7.93-8.00 (m, 3H), 7.82 (d, J = 8.0 Hz, 2H), 7.41 (d, J = 8.0 Hz, 3H), 7.18 (d, J = 16.0 Hz, 1H), 6.91 (s, 1H),

3.22(s, 3H). ^{13}C NMR (100 MHz, DMSO-d_6, ppm) 169.92, 160.67, 153.23, 150.86, 140.67, 139.05, 135.15, 130.40, 129.05, 128.59, 125.12, 123.27, 115.46, 114.09, 26.59. HRMS (ESI): *m*/*z* $[M + H]^+$ = calcd. for $C_{19}H_{15}F_2N_2O_2$, 341.1023; found 341.1021.

3.7 Synthesis of (4Z)-(3, 5-difluoro-4-hydroxybenzylidene)-1-methyl-2-((E)-2-(naphthalen-1-yl) vinyl)-1H-imidazol-5(4H)-one (DFHBNI).

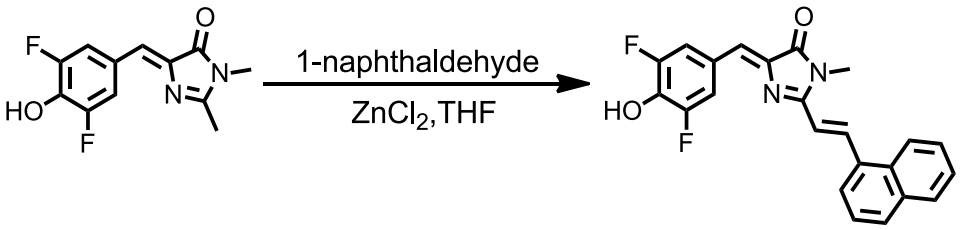

Compound **3a** (176 mg, 0.7 mmol), anhydrous zinc chloride (95 mg, 0.7 mmol), 1-naphthaldehyde (124.8 mg, 0.8 mmol) and THF (15 mL) were stirred at 80 ℃ for 6 h. After allowing the reaction to cool to room temperature, the crude product was purified by silica gel column chromatography (PE:EtOAc = 3:1, v/v) to afford compound DFHBNI (60.1 mg, yield 22%). ^{1}H NMR (400 MHz, DMSO-d_6, ppm) 10.21 (s, 1H), 8.21 (d, *J* = 8.0 Hz, 2H), 8.00 (d, *J* = 16.0 Hz, 1H), 7.86 (d, *J* = 8.0 Hz, 2H), 7.41-7.49 (m, 3H), 7.23 (d, *J* = 16.0 Hz, 1H), 7.00 (s, 1H), 6.90 (d, *J* = 8.0 Hz, 2H), 3.29 (s,3H). HRMS (ESI): *m*/*z* $[M + H]^+$ = calcd. for $C_{23}H_{17}F_2N_2O_2$ 391.1180; found 391.1176.

3.8 Synthesis of (4Z)-(3, 5-difluoro-4-hydroxybenzylidene)-2-((E)-4-(dimethylamino)styryl)-1-methyl-1H-imidazol-5(4H)-one (DFHBASI).

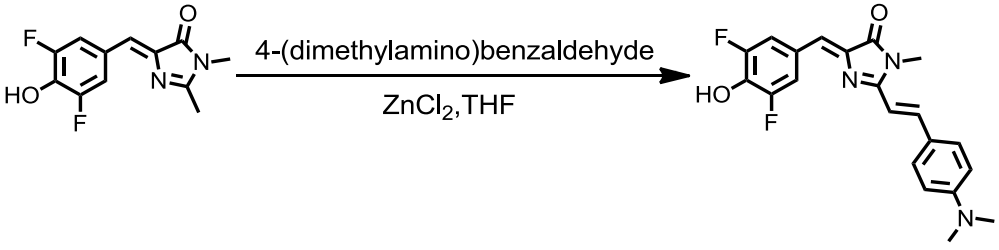

Compound **3a** (176 mg, 0.7 mmol), anhydrous zinc chloride (95 mg, 0.7 mmol), 4-(dimethylamino) benzaldehyde (119.2 mg, 0.8 mmol), and THF (15 mL) were stirred at 80 ℃ for 6 h. After allowing the reaction to cool to room temperature the crude product was purified by silica gel column chromatography (PE : EtOAc = 3:1, v/v) to

afford yellow solid (48.3 mg, yield 18%). ^{1}H NMR (400 MHz, DMSO-d_6, ppm) 10.06 (s, 1H), 8.13 (d, J = 8.0 Hz, 2H), 7.88 (d, J = 16.0 Hz, 1H), 7.66 (d, J = 12.0 Hz, 2H), 6.82-6.87 (m, 2H), 6.73 (d, J = 8.0 Hz, 2H), 3.21 (s, 3H), 2.98 (s, 6H). ^{13}C NMR (100 MHz, DMSO-d_6, ppm) 170.62, 159.96, 159.74, 152.04, 140.88, 137.74, 134.38, 130.51, 126.60, 124.13, 123.15, 116.28, 112.31, 108.09, 29.36, 29.74. HRMS (ESI): m/z [M + H]$^+$ = calcd. for $C_{21}H_{20}F_2N_3O_2$ 384.1445; found 384.1441.

3.9 Synthesis of (4Z)-(3, 5-difluoro-4-hydroxybenzylidene)-2-((1E, 3E)-4-(4-(dimethylamino) phenyl) buta-1, 3-dien-1-yl)-1-methyl-1H-imidazol-5(4H)-one (DFHBAPBI).

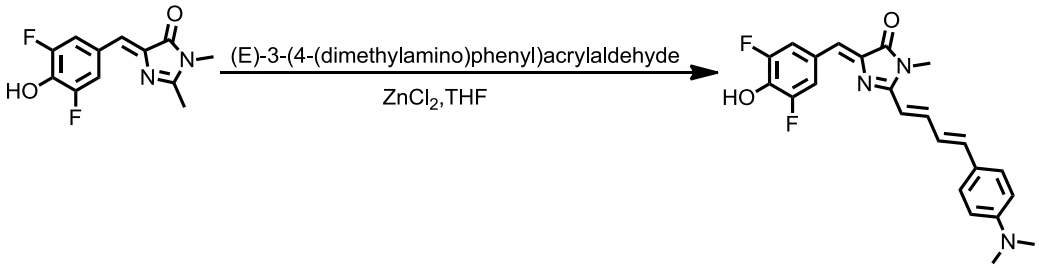

Compound **3a** (176 mg, 0.7 mmol), anhydrous zinc chloride (95 mg, 0.7 mmol), (E)-3-(4-(dimethylamino) phenyl) acrylaldehyde (140.1 mg, 0.8 mmol), and THF (15 mL) were stirred at 80 ℃ for 6 h. After allowing the reaction to cool to room temperature the crude product was purified by silica gel column chromatography (PE:EtOAc = 3:1, v/v) to afford a yellow solid (34.3 mg, yield 12%). ^{1}H NMR (400 MHz, DMSO-d_6, ppm) 8.35-8.43 (m, 1H), 8.05 (dd, J_1 = 12.0 Hz, J_2 = 8.0 Hz, 2H), 7.81 (q, J = 8.0 Hz, 1H), 7.49 (q, J = 8.0 Hz, 2H), 6.99-7.17 (m, 2H), 6.73-6.87 (m, 2H), 6.08-6.58 (m, 1H), 3.18 (s, 3H), 3.06 (s, 6H).

3.10 Synthesis of (4Z)-(4-hydroxybenzylidene)-1-methyl-2-((E)-styryl)-1H-imidazol-5(4H)-one (1b)

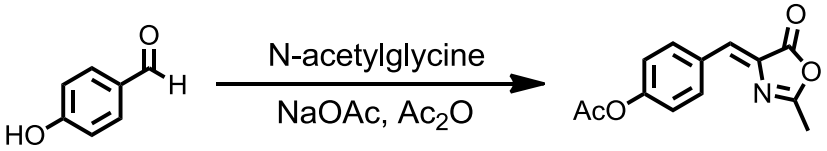

N-Acetylglycine (11.7 g, 1.0 mol), anhydrous sodium acetate (8.2 g, 0.1 mol), 4-hydroxybenzaldehyde (12.2 g, 0.1 mol), and acetic anhydride (100 mL) were stirred at 120 ℃ under argon for 4 h. The resulting crystalline solid was washed with a small amount of cold ethanol, hot water and dried to afford a yellow solid (21.28 g, yield 70%). The product was used for the next step without purification.

3.11 Synthesis of (4Z)-(3, 5-difluoro-4-hydroxybenzylidene)-1, 2-dimethyl-1H-imidazol-5(4H)-one (2b)

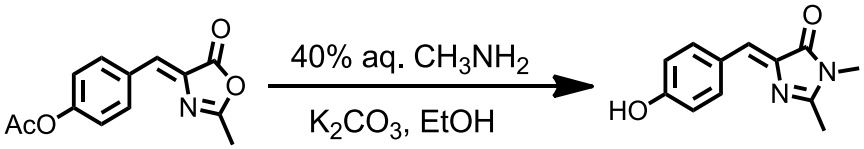

Compound **1b** (2.81 g, 0.01mol), potassium carbonate (1.97 g, 0.014 mol), 40% aqueous methylamine (3 mL), and ethanol (40 mL) were stirred at 120 ℃ for 5 h. The mixture was cooled to room temperature, and the precipitate was filtered and washed briefly with cold ethanol. Then the precipitate was re-dissolved in a 1:1 mixture of ethyl acetate and aqueous sodium acetate solution (500 mM, pH 3.0). The organic layer was separated, dried with anhydrous magnesium sulfate and solvent was evaporated in vacuums to afford an orange solid (1.81 g, yield 72%). ^{1}HNMR (400 MHz, CD_3OD, ppm) 10.11 (s, 1H), 8.08 (d, J = 8 Hz, 2H), 6.89 (s, 1H), 6.84 (d, J = 4Hz, 2H), 3.09 (s, 3H), 2.33 (s, 3H). ^{13}CNMR (100 MHz, CD_3OD, ppm) 169.72, 162.12, 159.43, 136.10, 133.78, 125.24, 125.02, 115.43, 26.03, 15.46.

3.12 Synthesis of (4Z)-(4-hydroxybenzylidene)-1-methyl-2-((E)-styryl)-1H-imidazol-5(4H)-one (HBSI).

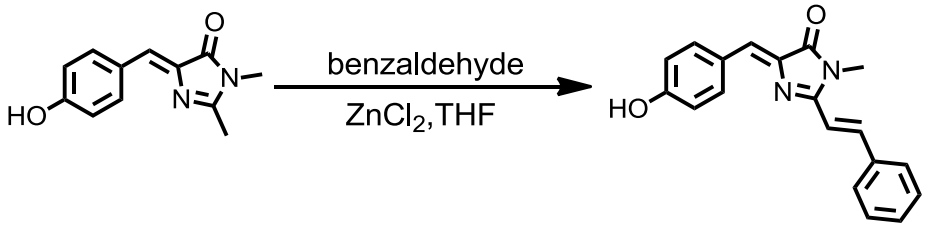

Compound **2b** (176 mg, 0.7 mmol), anhydrous zinc chloride (95 mg, 0.7 mmol), benzaldehyde (84.8 mg, 0.8 mmol), and THF (15 mL) were stirred at 80 ℃ for 6 h.

After allowing the reaction to cool to room temperature the crude product was purified by silica gel column chromatography (PE: EtOAc = 5:1, v/v) to afford a yellow solid (85.1 mg, yield 40%). ^{1}H NMR (400 MHz, DMSO-d_6, ppm) 10.19 (s, 1H), 8.20 (d, J = 8.0 Hz, 2H,), 7.99 (d, J = 16.0 Hz, 1H), 7.85 (d, J = 4.0 Hz, 2H), 7.42-7.48 (m, 3H), 7.21 (d, J = 16.0 Hz, 1H), 6.98 (s, 1H), 6.88 (d, J = 8.0 Hz, 2H), 3.27 (s, 3H). ^{13}C NMR (100 MHz, DMSO-d_6, ppm) 169.97, 159.77, 158.74, 139.44, 136.92, 135.22, 134.50, 129.97, 128.88, 128.23, 125.97, 125.83, 115.89, 114.14, 26.37. HRMS (ESI): m/z [M + H]$^+$ = calcd. for $C_{19}H_{17}N_2O_2$ 305.1212; found 305.1207.

3.13 Synthesis of (4Z)-(4-hydroxybenzylidene)-1-methyl-2-((E)-2-(naphthalen-1-yl) vinyl)-1H-imidazol-5(4H)-one (HBNI).

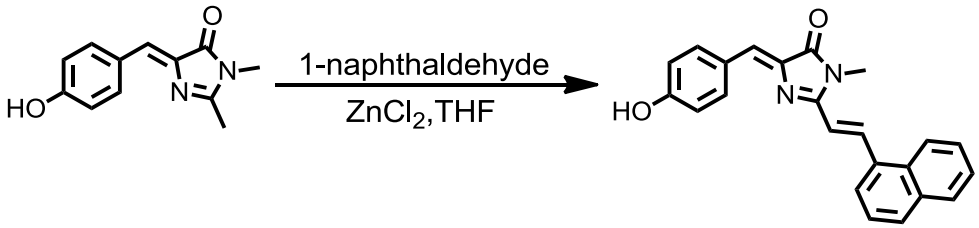

Compound **2b** (176 mg, 0.7 mmol), anhydrous zinc chloride (95 mg, 0.7 mmol), 1-naphthaldehyde (124.8 mg, 0.8 mmol), and THF (20 mL) were stirred at 80 ℃ for 4 h. After allowing the reaction to cool to room temperature the crude product was purified by silica gel column chromatography (PE:EtOAc = 3:1, v/v) to afford a yellow solid (103.1mg, yield 39%). ^{1}H NMR (400 MHz, DMSO-d_6, ppm) 10.21 (s, 1H), 8.77 (d, J = 16.0 Hz, 1H), 8.36 (d, J = 8.0 Hz, 1H), 8.25 (d, J = 8.0 Hz, 2H), 8.17 (d, J = 8.0 Hz, 1H), 8.04 (t, J = 8.0 Hz ,2H), 7.62-7.69 (m, 3H), 7.30 (d, J = 16.0 Hz, 1H), 7.04(s, 1H), 6.92 (d, J = 8.0 Hz, 2H), 3.33 (s, 3H). ^{13}C NMR (100 MHz, DMSO-d_6, ppm) 170.08, 159.95, 158.83, 136.98, 135.48, 134.71, 133.47, 132.12, 130.92, 130.37, 128.86, 127.28, 126.47, 126.41, 125.91, 125.84, 125.42, 123.29, 116.95, 116.07, 26.55. HRMS (ESI): m/z [M + H]$^+$ = calcd. for $C_{23}H_{19}N_2O_2$ 355.1368; found 355.1364.

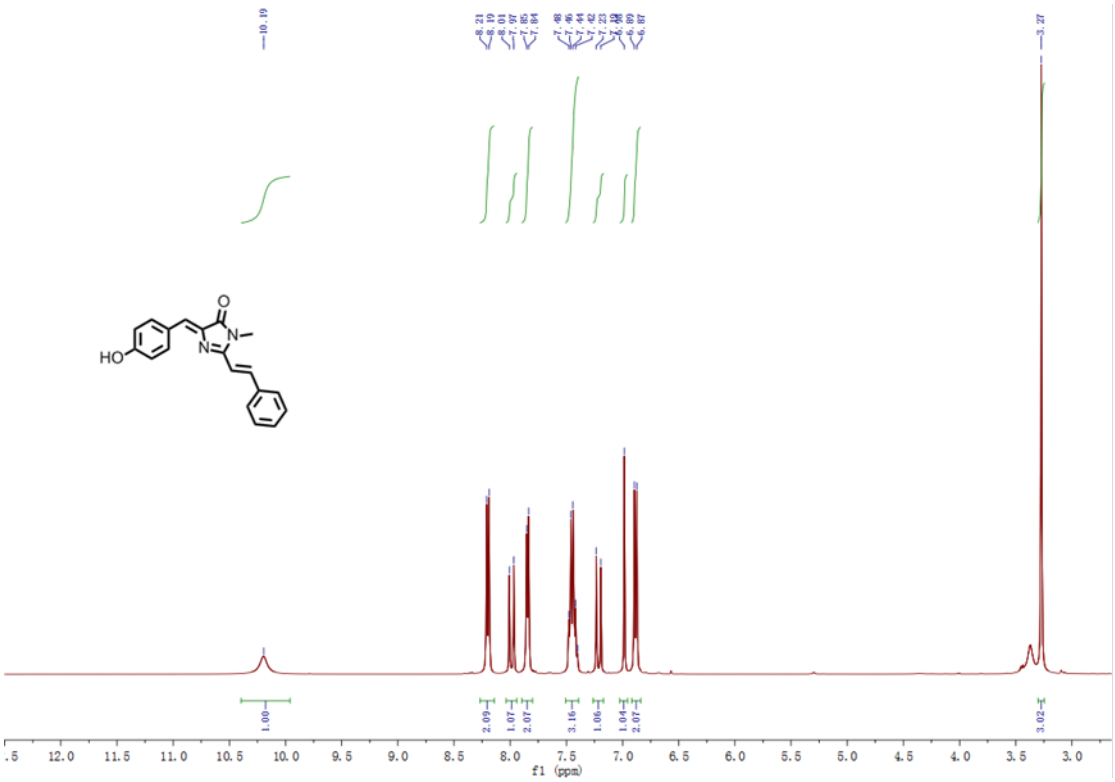
10.19
8.21
8.19
8.01
7.97
7.85
7.84
7.48
7.46
7.44
7.42
7.23
7.21
6.89
6.87
3.27
HO
O
N
1.00
2.09
1.07
2.07
3.16
1.06
1.04
2.07
3.02
f1 (ppm)

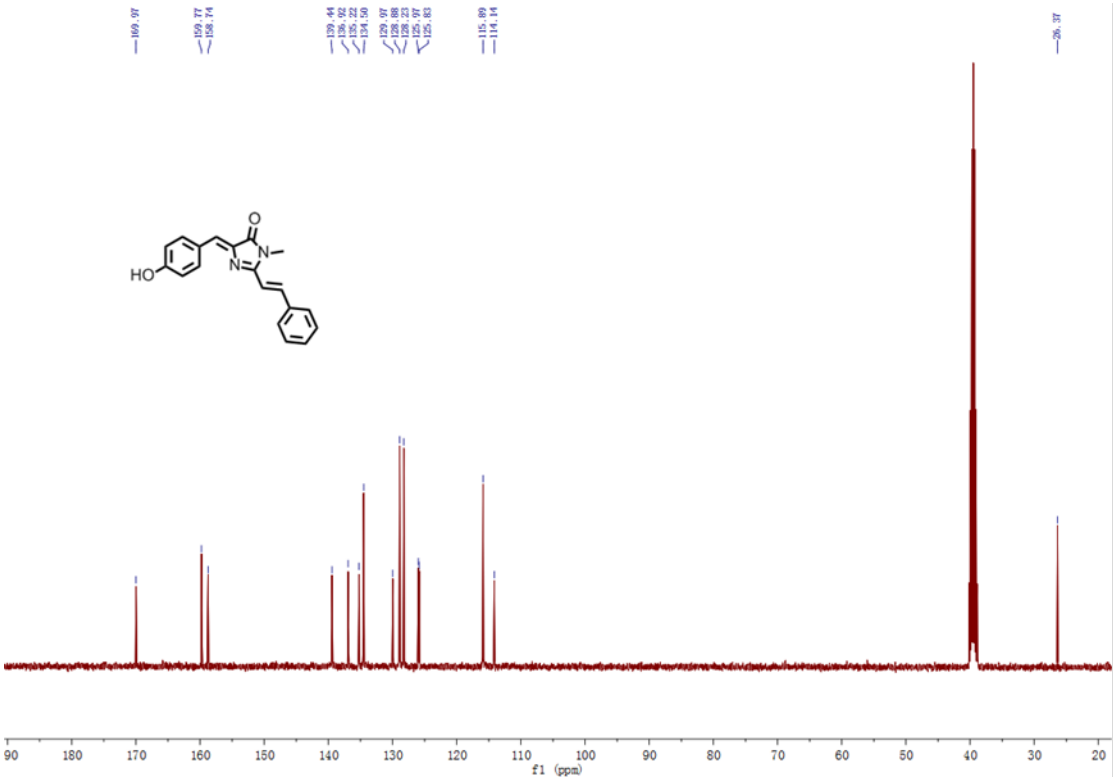
169.97
159.77
158.74
139.44
136.92
135.22
134.50
129.97
128.88
128.23
125.97
125.83
115.89
114.14
26.37
HO
O
N
f1 (ppm)

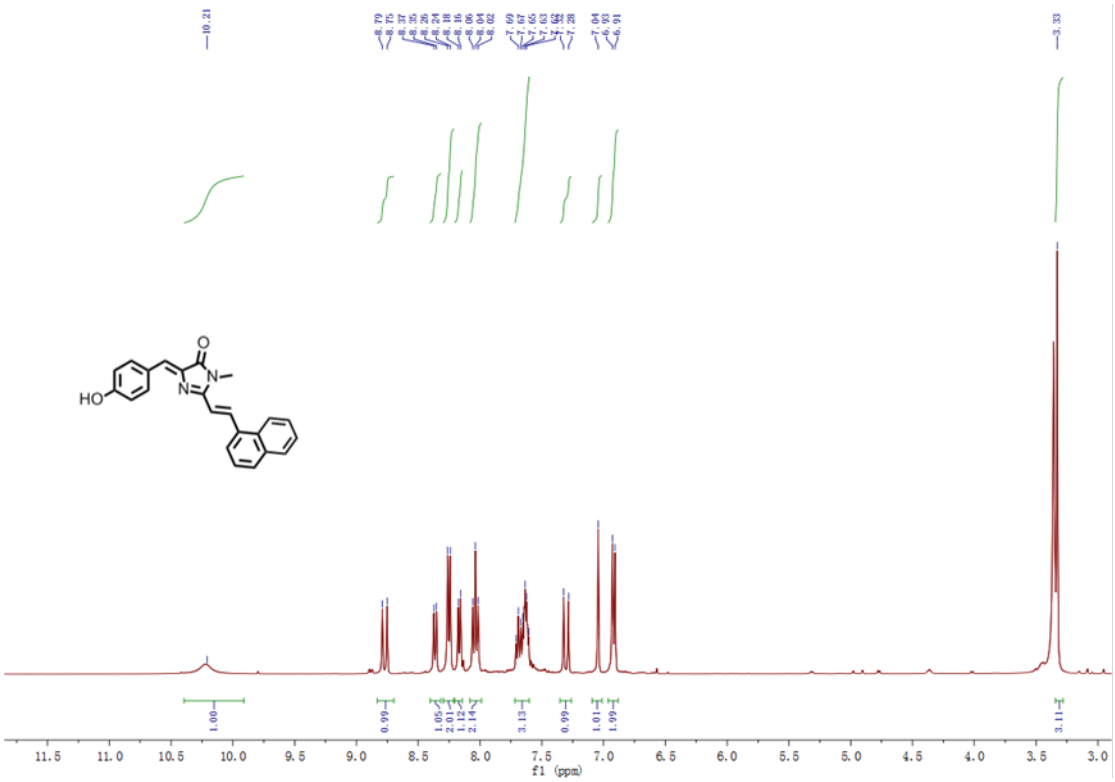
10.21
8.79
8.75
8.37
8.35
8.26
8.24
8.18
8.16
8.06
8.04
8.02
7.69
7.67
7.65
7.63
7.62
7.55
7.28
7.04
6.95
6.91
3.33
HO
O
N
1.00
0.99
1.05
2.01
1.12
2.14
3.13
0.99
1.01
1.99
3.11
11.5
11.0
10.5
10.0
9.5
9.0
8.5
8.0
7.5
7.0
6.5
6.0
5.5
5.0
4.5
4.0
3.5
3.0
f1 (ppm)

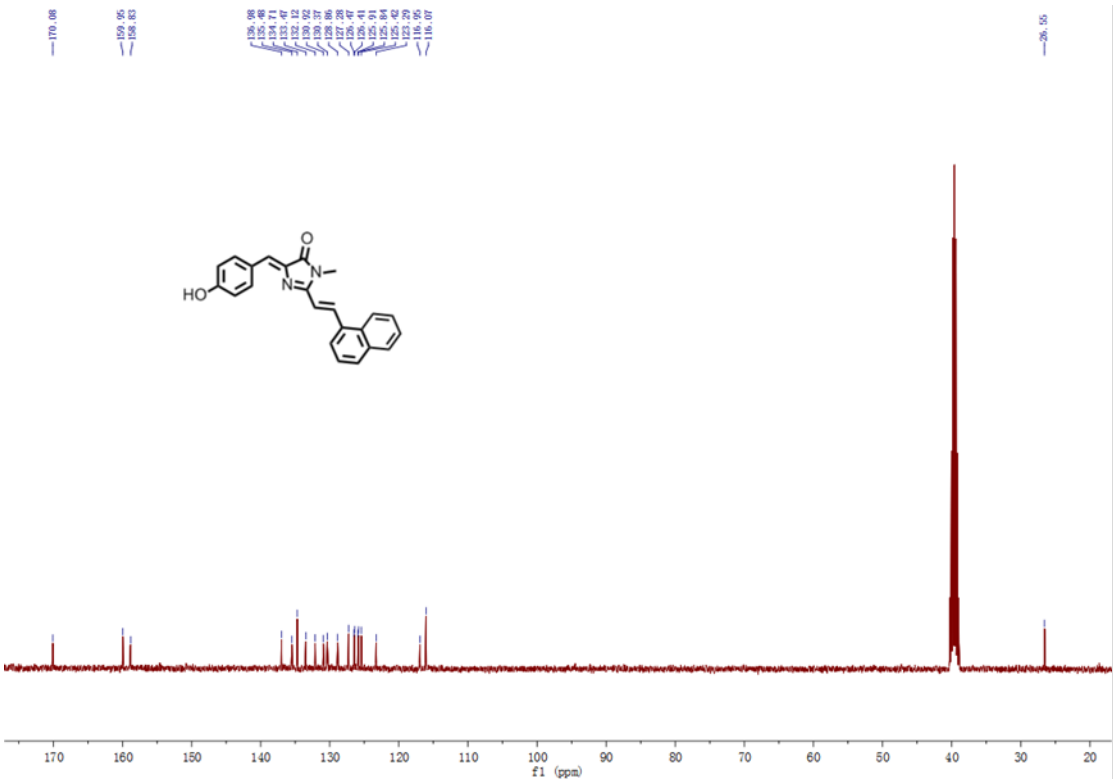
170.08
159.95
158.83
136.98
135.48
134.71
133.47
132.12
130.92
130.37
128.86
127.28
126.49
126.41
125.91
125.84
125.62
123.29
116.95
116.07
26.55
HO
O
N
170
160
150
140
130
120
110
100
90
80
70
60
50
40
30
20
f1 (ppm)

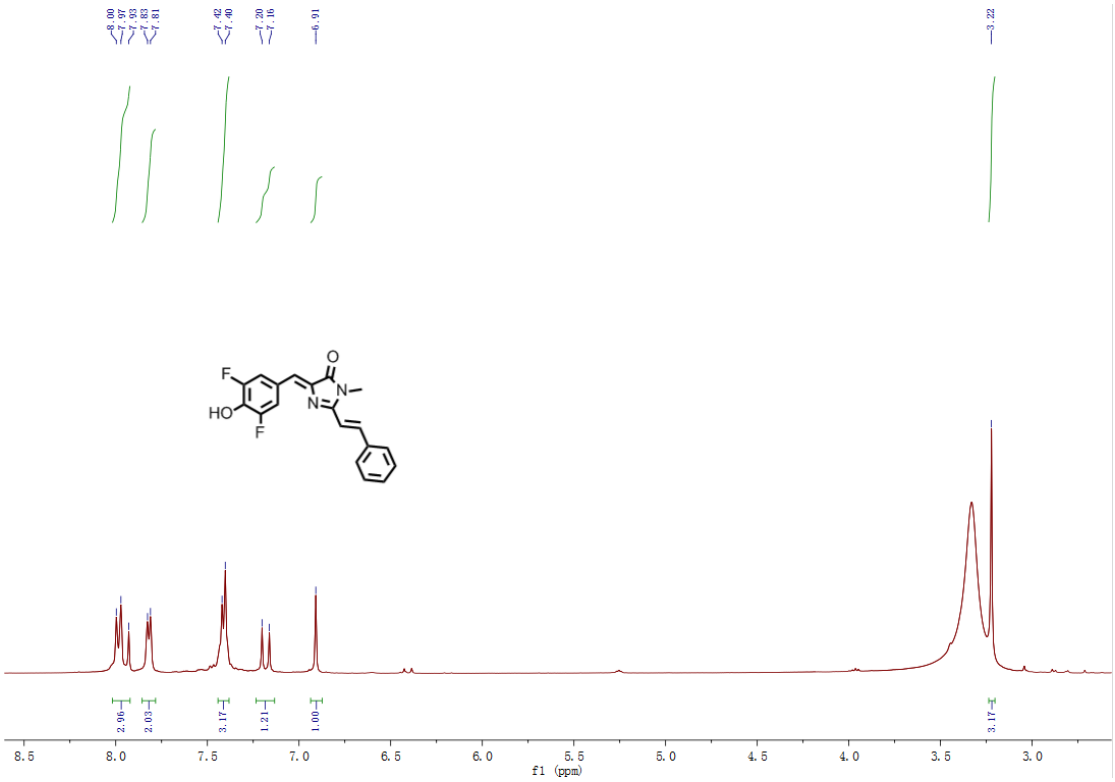
8.00
7.97
7.93
7.83
7.81
7.42
7.40
7.20
7.16
6.91
3.22
F
HO
F
O
N
N
2.96
2.03
3.17
1.21
1.00
3.17
8.5
8.0
7.5
7.0
6.5
6.0
5.5
5.0
4.5
4.0
3.5
3.0
f1 (ppm)

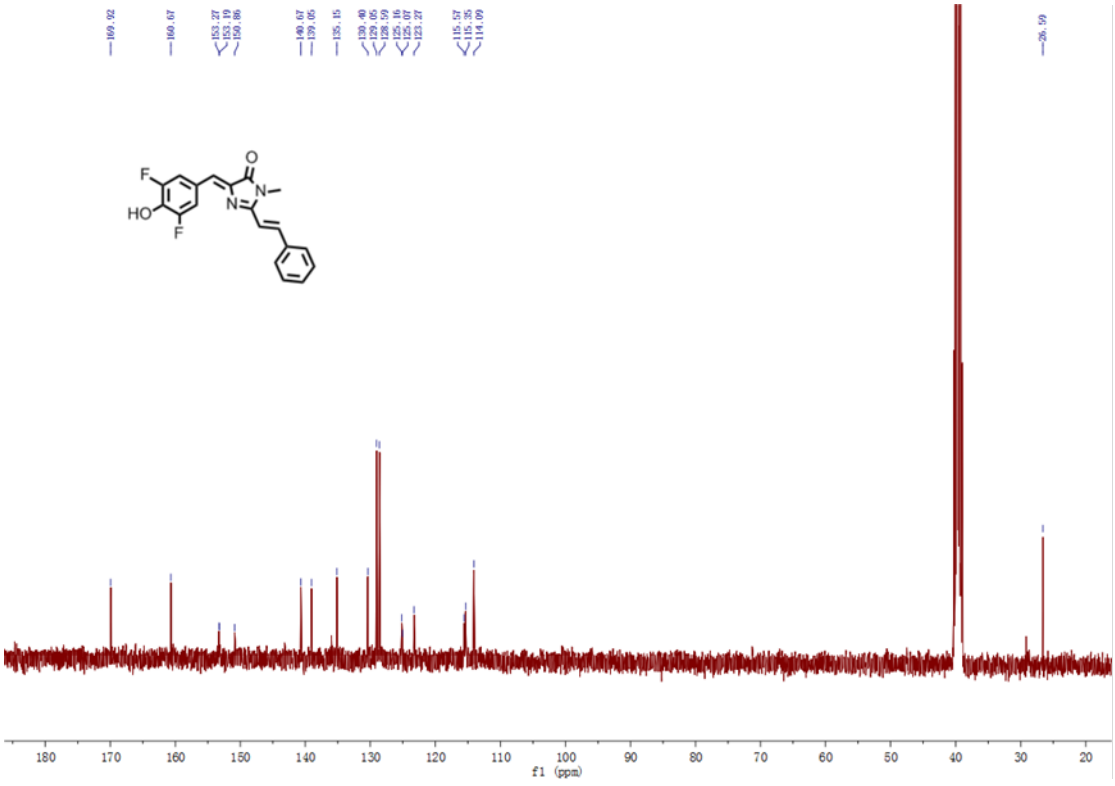
169.92
160.67
153.27
151.19
150.86
140.67
139.05
135.15
130.40
129.05
128.59
125.16
125.07
123.27
115.57
115.35
114.99
26.59
F
HO
F
O
N
N
180
170
160
150
140
130
120
110
100
90
80
70
60
50
40
30
20
f1 (ppm)

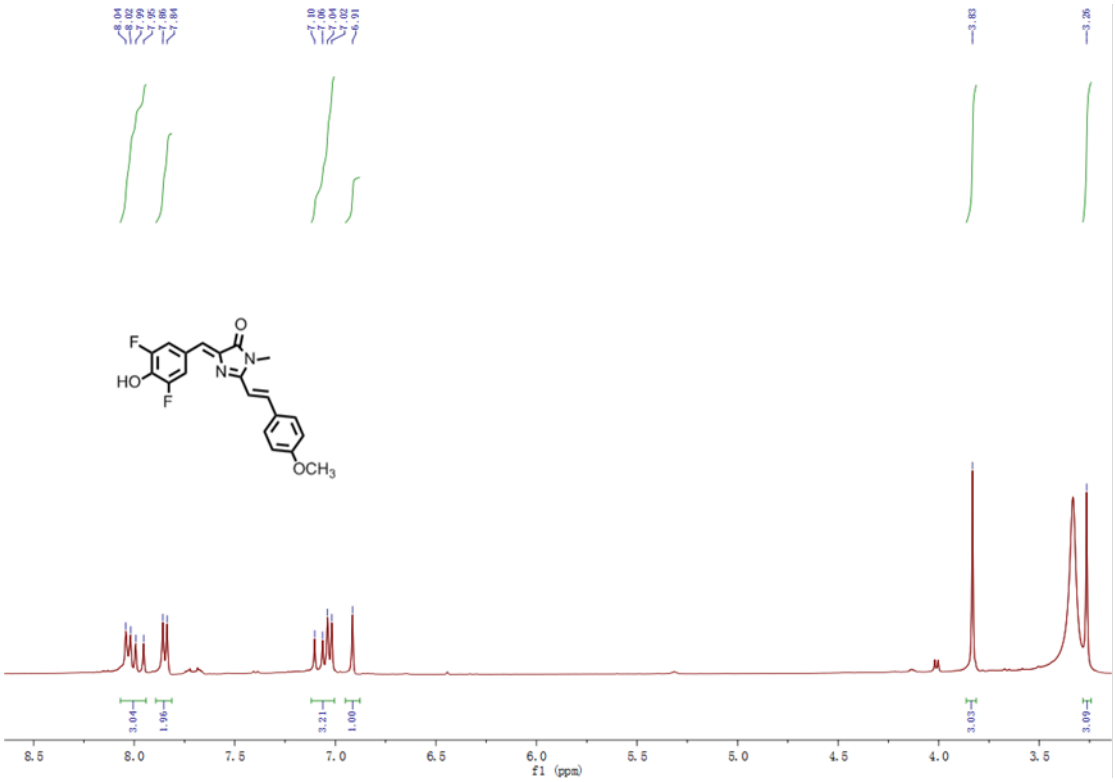
F
HO
F
O
N
N
OCH3
8.5
8.0
7.5
7.0
6.5
6.0
5.5
5.0
4.5
4.0
3.5
f1 (ppm)

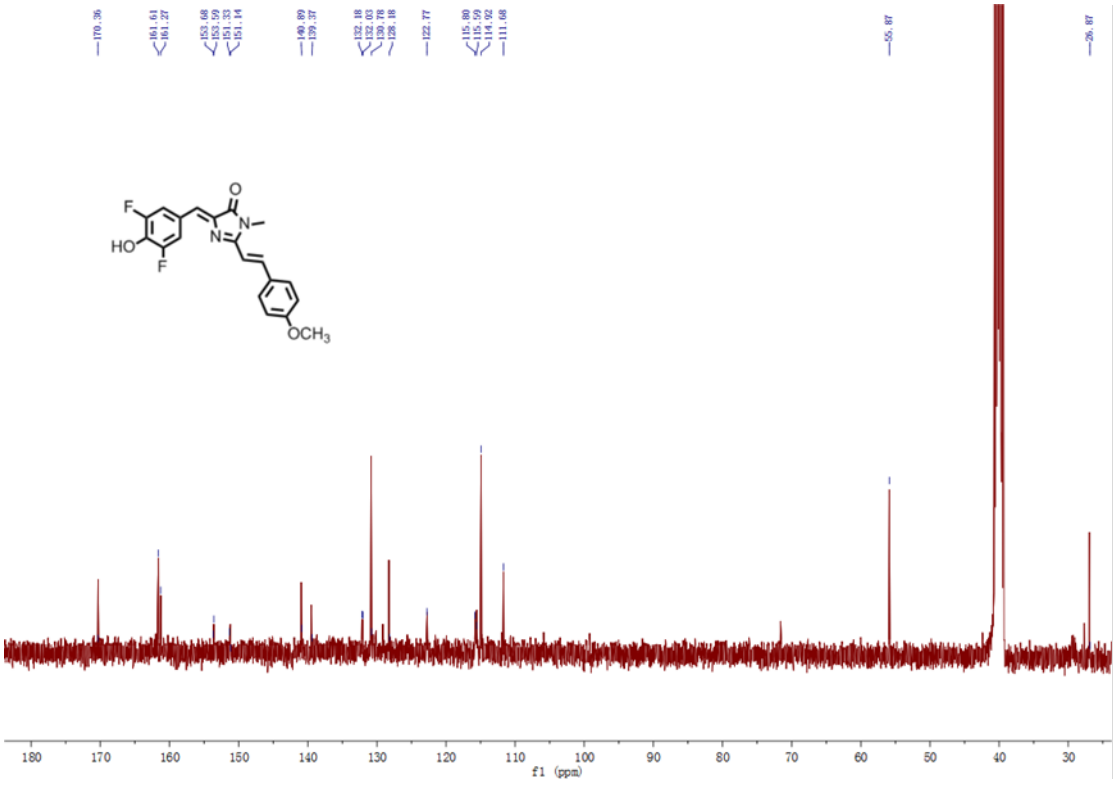
F
HO
F
O
N
N
OCH3
180
170
160
150
140
130
120
110
100
90
80
70
60
50
40
30
f1 (ppm)

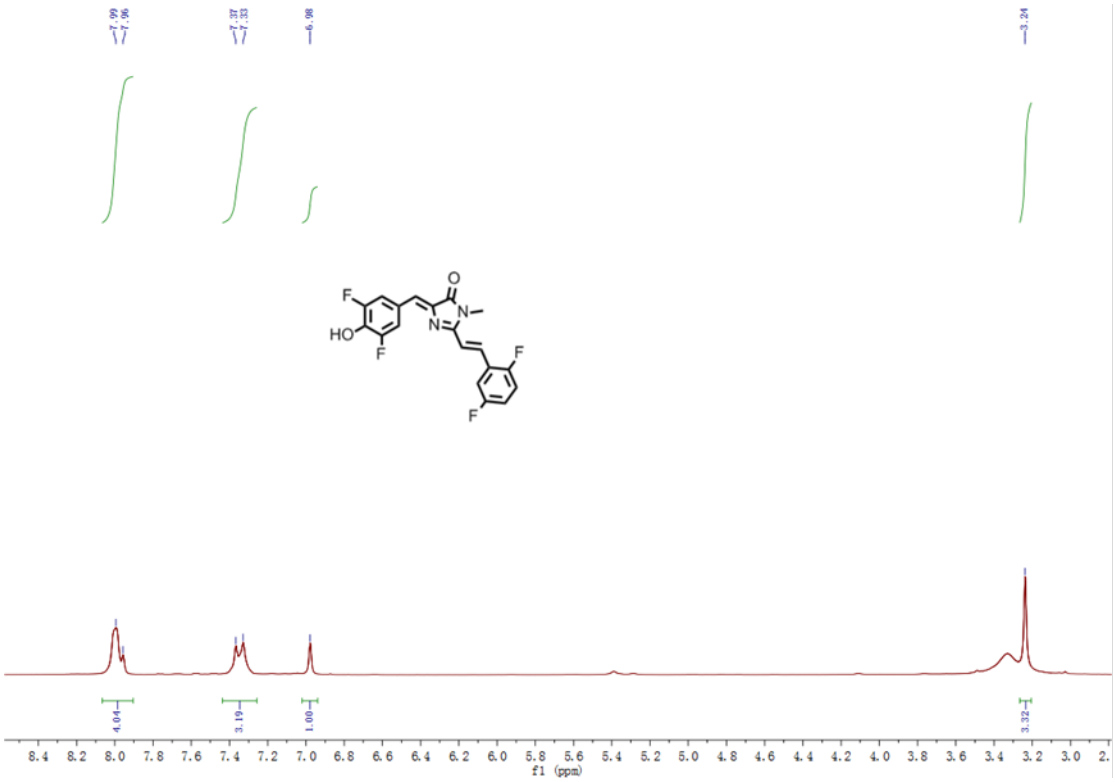
7.99
7.96
7.37
7.33
6.98
3.24
F
HO
F
O
N
N
F
F
4.04
3.19
1.00
3.32
f1 (ppm)

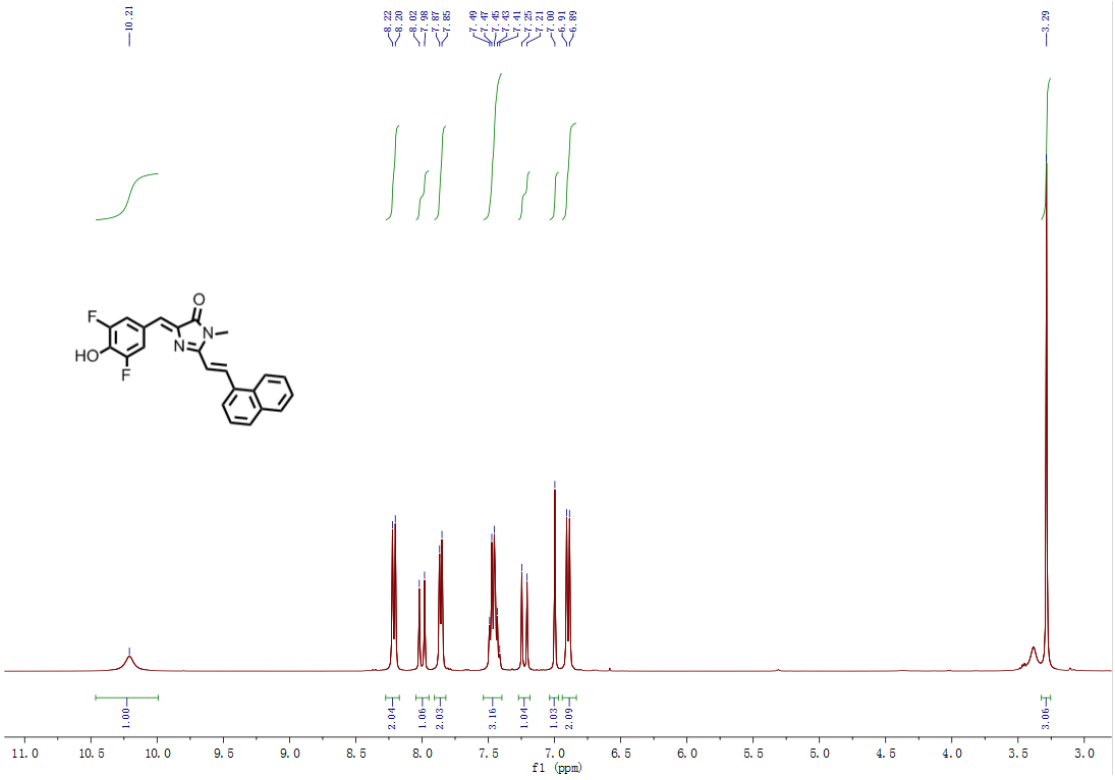
10.21
8.22
8.20
8.02
7.98
7.87
7.85
7.49
7.47
7.45
7.43
7.41
7.25
7.21
7.00
6.91
6.89
3.29
F
HO
F
O
N
N
1.00
2.04
1.06
2.03
3.16
1.04
1.03
2.09
3.06
f1 (ppm)

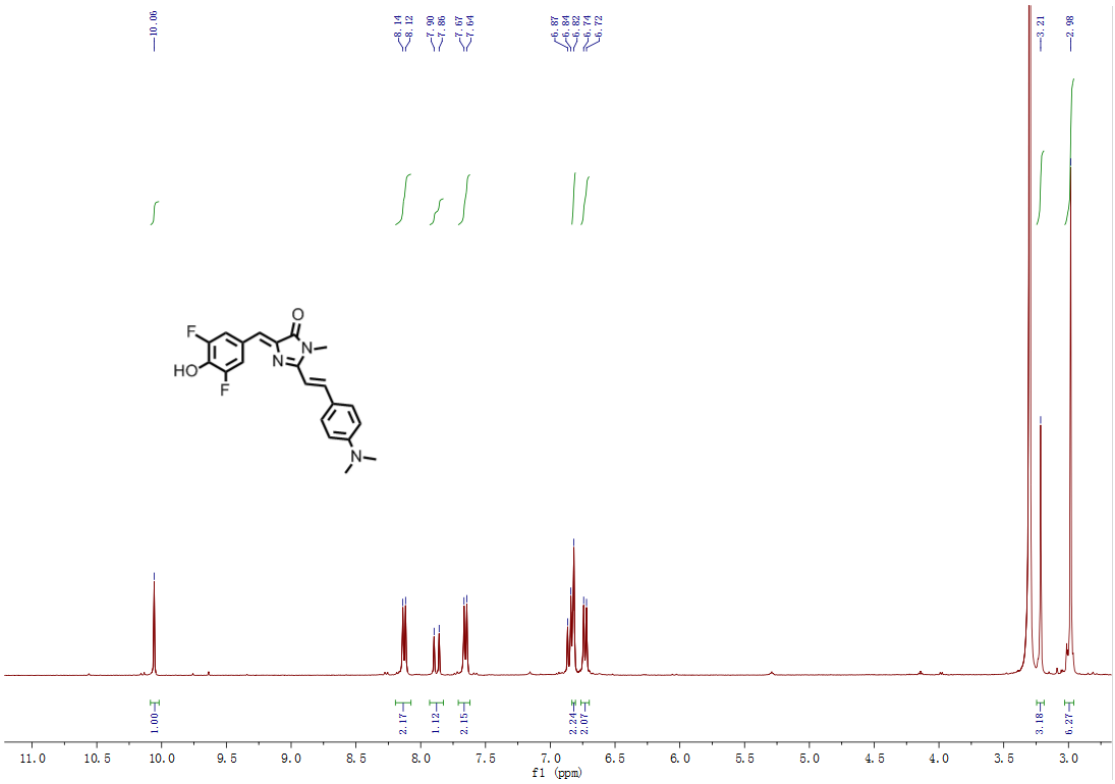
10.06
8.14
8.12
7.90
7.86
7.67
7.64
6.87
6.84
6.82
6.74
6.72
3.21
2.98
F
HO
F
O
N
N
N
1.00
2.17
1.12
2.15
2.24
2.07
3.18
6.27
11.0
10.5
10.0
9.5
9.0
8.5
8.0
7.5
7.0
6.5
6.0
5.5
5.0
4.5
4.0
3.5
3.0
f1 (ppm)

4. References.

1] N. S. Makarov, M. Drobizhev, A. Rebane. (2008) Two-photon absorption standards in the 550-1600 nm excitation wavelength range. *Opt. Express*., **16**, 4029-4047.

[2] D. Magde, G. E. Rojas, P. G. Seybold. (1999) Solvent Dependence of the Fluorescence Lifetimes of Xanthene Dyes. *Photochem. Photobiol.*, **70**, 737-744.

[3] L. Zhang, J. C. Er, K. K. Ghosh, W. J. Chung, J. Yoo, W. Xu, W. Zhao, A. T. Phan, Y. T. Chang. (2014) Discovery of a Structural-Element Specific G-Quadruplex ‘‘Light-Up’’ Probe. *Sci. Rep.*, **4**, 3776.

[4] V. Kuryavyi, L.A. Cahoon, H.S. Seifert, D. J. Patel. (2012) RecA-binding pilE G4 sequence essential for pilin antigenic variation forms monomeric and 5' end-stacked dimeric parallel G-quadruplexes. *Structure*, **20**, 2090–2102.

[5] H.M. Berman, J. Westbrook, Z. Feng, G. Gilliland, T.N. Bhat, H. Weissig, I.N. Shindyalov, P.E. Bourne. (2000) The Protein Data Bank. *Nucleic Acids Res*., **28**, 235–242.

[6] G. M. Morris, R. Huey, W. Lindstrom, M. F. Sanner, R. K. Belew, D. S. Goodsell, A. J. Olson. (2009**)** AutoDock4 and AutoDockTools4: Automated Docking with Selective Receptor Flexibility. *J. Comput. Chem.*, **30**, 2785–2791.

[7] K. Vanommeslaeghe, E. Hatcher, C. Acharya, S. Kundu, S. Zhong, J. Shim, E. Darian, O. Guvench, P. Lopes, I. Vorobyov, A. D. MacKerell Jr. (2010) CHARMM General Force Field: A Force Field for Drug-Like Molecules Compatible with the CHARMM All-Atom Additive Biological Force Fields. *J. Comput. Chem.*, **31**, 671–690.

[8] K. Hart, N. Foloppe, C. M. Baker, E. J. Denning,L. Nilsson, A. D. MacKerell Jr. (2012) Optimization of the CHARMM Additive Force Field for DNA: Improved Treatment of the BI/BII Conformational Equilibrium. *J. Chem. Theory Comput.*, **8**, 348–362.

[9] K. N. Luu, A. T. Phan, V.V. Kuryavyi, L. Lacroix, D. J. Patel. (2006) Structure of the Human Telomere in K^+ Solution: An Intramolecular (3 + 1) G-Quadruplex Scaffold. *J. Am. Chem. Soc.*, **128**, 9963–9970.

[10] J. Lietard, H. Abou Assi, I. Gomez-Pinto, C. Gonzalez, M. M. Somoza, M. J. Damha. (2017) Mapping the affinity landscape of Thrombin-binding aptamers on 2'F-ANA/DNA chimeric G-Quadruplex microarrays. *Nucleic Acids Res*., **45**, 1619–1632.

[11] W. Im, D. Beglov, B. Roux. (1998) Continuum Solvation Model: computation of electrostatic forces from numerical solutions to the Poisson-Boltzmann equation. *Comput. Phys. Commun.*, **111**, 59–75.

[12] The PyMOL Molecular Graphics System, Version 1.3, Schrödinger, LLC.

[13] T. Yanai, D.Tew, N. Handy. (2004) A new hybrid exchange–correlation functional using the Coulomb-attenuating method (CAM-B3LYP). *Chem. Phys. Lett.*, **393**, 51–57.

[14] R. Krishnan, J. S. Binkley, R. Seeger, J. A. Pople. (1980) Self-consistent molecular orbital methods. XX. A basis set for correlated wave functions. *J. Chem. Phys*., **72**, 650–654.

[15] E. Runge, E. K. U. Gross. (1984) Density-functional theory for time-dependent systems. *Phys. Rev. Lett.*, **52**, 997–1000.

[16] E. K. U. Gross, W. Kohn. (1990) Time-dependent density-functional theory. *Adv. Quantum Chem.*, **21**, 255–291.

[17] M. J. Frisch, G. W. Trucks, H. B. Schlegel, G. E.Scuseria, M. A. Robb, J. R. Cheeseman, G. Scalmani, V. Barone, B. Mennucci, G. A. Petersson et al. Gaussian 09, Revision A.1; Gaussian, Inc.: Wallingford, CT, 2009.

[18] W. Humphrey, A. Dalke, K. Schulten. (1996) VDM: visual molecular dynamics. *J. Mol. Graphics*., **14**, 33–38.

[19] E. M. M. Manders, F. J. Verbeek, J. A. Aten. (1993) Measurement of co-localization of objects indual-colour confocal images. *J. Microsc.*, **169**, 375–382.

[20] N. J. Lawrence, L. A. Hepworth, D. Rennison, A. T.Mcgown, J. A.Hadfield. (2003) Synthesis and anticancer activity of fluorinated analogues of combretastatin A-4. *J. Fluor. Chem.*, **123**, 101–108.

[21] W. Song, R. L. Strack, N. Svensen, S. R. Jaffrey. (2014) Plug-and-Play Fluorophores Extend the Spectral Properties of Spinach. *J. Am. Chem. Soc.*, **136**, 1198–1201.